



# CHORUS

This is the accepted manuscript made available via CHORUS. The article has been published as:

## Dynamics of correlation spreading in low-dimensional transverse-field Ising models

Ryui Kaneko and Ippei Danshita

Phys. Rev. A **108**, 023301 — Published 1 August 2023

DOI: [10.1103/PhysRevA.108.023301](https://doi.org/10.1103/PhysRevA.108.023301)

# Dynamics of correlation spreading in low-dimensional transverse-field Ising models

Ryui Kaneko\* and Ippei Danshita†

*Department of Physics, Kindai University, Higashi-Osaka, Osaka 577-8502, Japan*

(Dated: July 19, 2023)

We investigate the dynamical spreading of spatial correlations after a quantum quench starting from a magnetically disordered state in the transverse-field Ising model at one (1D) and two spatial dimensions (2D). We analyze specifically the longitudinal and transverse spin-spin correlation functions at equal time with use of several methods. From the comparison of the results in 1D obtained by the linear spin-wave approximation (LSWA) and those obtained by the rigorous analytical approach, we show that the LSWA can asymptotically reproduce the exact group velocity in the limit of strong transverse fields while it fails to capture the detailed time dependence of the correlation functions. By applying the LSWA to the 2D case, in which the rigorous analytical approach is unavailable, we estimate the propagation velocity to be  $Ja/(2\hbar)$  at the strong-field limit, where  $J$  is the Ising interaction and  $a$  is the lattice spacing. We also utilize the tensor-network method based on the projected-entangled pair states for 2D and quantitatively compute the time evolution of the correlation functions for a relatively short time. Our findings provide useful benchmarks for quantum simulation experiments of correlation spreading and theoretical refinement of the Lieb-Robinson bound in the future.

## I. INTRODUCTION

Neutral atoms trapped in optical-tweezer arrays are promising platforms for analog quantum simulations [1–3]. The controllability of individual atoms with laser pulses and of interatomic interactions via Rydberg excitations enables one to realize fast and high-fidelity quantum operations. Recent rapid technological developments allow for manipulating many Rydberg atoms in large arrays [4–6] and investigating the ground state of quantum lattice systems experimentally [7–15]. Such experiments have also stimulated theoretical research on fundamental quantum many-body systems. For instance, the ground-state phase diagrams of the transverse-field Ising model and those of its strong Ising interaction limit, the PXP model, have been intensively examined using the quantum Monte Carlo method [16–19].

Rydberg-atom arrays have also given the opportunity to study the nonequilibrium dynamics of isolated quantum many-body systems, which are hard to simulate numerically with classical computers. In particular, the correlation-spreading dynamics of quantum Ising models [16, 20] is one of the intriguing topics that is likely to be further addressed. At present, experiments with more than 200 Rydberg atoms are feasible [4–6], allowing one to study unprecedentedly large lattice systems in one (1D) and two spatial dimensions (2D).

These recent experiments on long-time dynamics in quantum many-body systems have motivated us to quantitatively calculate the velocity of the correlation propagation, which will serve as useful references for future

experiments. In general, there are two kinds of propagation velocities for correlation spreading dynamics; one is the phase velocity and the other is the group velocity. The former can be captured by the first peak of the wave packet, whereas the latter can be extracted by the envelope of the wave packet. The group velocity is bounded from above in non-relativistic quantum systems, and this upper limit is known as the Lieb-Robinson bound [21, 22].

While significant progress has been made concerning rigorous inequalities related to the Lieb-Robinson bound, such inequalities do not necessarily offer practical reference values for experiments. Usually, the Lieb-Robinson bound is intended to provide general conditions for arbitrary correlations. Consequently, the bound can be too loose and sometimes meaningless when examining the propagation velocity of particular correlation functions that are measurable in experiments. With this in mind, the Lieb-Robinson bound has been improved very recently [23]; however, their method still gives a looser bound than the exact solution if it is available.

In some cases, direct numerical simulations on classical computers would give much more detailed information about correlation spreading than rigorous inequalities for the Lieb-Robinson bound. Such numerical data would also strengthen the validity of experimental findings through cross-checking experimental and theoretical results. Indeed, many numerical efforts have been made to calculate the quench or sweep dynamics in 1D and 2D. These attempts include the time-dependent variational Monte Carlo method with the Slater-Jastrow wave function [24] and with more sophisticated neural-network wave functions [25–31], the form factor expansions [32], the numerical linked-cluster expansion [33–35], the tensor-network method based on matrix product states (MPS) [36–39], and that based on projected entangled pair states (PEPS) [28, 40–45].

In this paper, we study quench dynamics in the transverse-field Ising model on a chain in 1D and that

---

\* Current address: Waseda Research Institute for Science and Engineering, Waseda University, Shinjuku, Tokyo 169-8555, Japan; Current address: Department of Engineering and Applied Sciences, Sophia University, Chiyoda, Tokyo 102-8554, Japan; [ryuikaneko@aoni.waseda.jp](mailto:ryuikaneko@aoni.waseda.jp)

† [danshita@phys.kindai.ac.jp](mailto:danshita@phys.kindai.ac.jp)

on a square lattice in 2D by using several methods, including the tensor-network method based on PEPS and the linear spin-wave approximation (LSWA). We take the initial state to be the magnetically disordered product state, which is the ground state in the strong-field limit, and calculate time evolution of spin-spin correlations at equal time after a sudden quench of the transverse field. We focus on the quench within a parameter region where the ground state is magnetically disordered. We extract the group velocity of the correlation propagation from the spin-spin correlations for several values of the transverse field. In the 1D case, we show that the group velocity extracted from the LSWA results asymptotically approaches that extracted from the rigorous analytical results with increasing the transverse field, while the agreement in the time dependence of the correlation functions is limited to a short time before the first peak appears. Our results indicate that the LSWA can quantitatively predict the propagation velocity as long as the final transverse field is sufficiently strong. In the 2D case, using the LSWA, we estimate the group velocity to be  $Ja/(2\hbar)$ , where  $J$  is the Ising interaction and  $a$  is the lattice spacing. We use the PEPS method in a complementary way to perform more quantitative calculations on the time evolution of the correlation functions for a relatively short time.

This paper is organized as follows: In Sec. II, we introduce the model and all the analytical and numerical methods used in the present study. In Secs. III and IV, we present the time-dependent spin-spin correlation functions and extract the corresponding group velocity in 1D and 2D, respectively. We discuss the relation between our propagation velocity and the Lieb-Robinson bound proposed recently, and draw our conclusions in Sec. V. For simplicity, we set  $\hbar = 1$  throughout this paper.

## II. MODEL AND METHODS

We consider the transverse-field Ising model with the periodic boundary condition defined as

$$\hat{H} = -J \sum_{\langle i,j \rangle} \hat{S}_i^z \hat{S}_j^z - \Gamma \sum_i \hat{S}_i^x, \quad (1)$$

where  $\hat{S}_i^z$  and  $\hat{S}_i^x$  correspond to the  $z$  and  $x$  components of the  $S = 1/2$  Pauli spin,  $J$  represents the strength of the spin exchange interaction, and  $\Gamma$  represents the strength of the transverse field. The symbol  $\langle i,j \rangle$  means that the sum is taken over nearest-neighbor sites. We focus on the ferromagnetic spin exchange interaction ( $J > 0$ ) on a chain in 1D and that on a square lattice in 2D. Both ferromagnetic and antiferromagnetic models are equivalent under appropriate unitary transformations for bipartite lattices. The ground state is ordered (disordered) for  $\Gamma < \Gamma_c$  ( $\Gamma > \Gamma_c$ ), where  $\Gamma_c$  is the transition point given as  $\Gamma_c/J = 1/2$  [46] in 1D and  $\Gamma_c/J \approx 1.522$  [17, 47, 48] in 2D. Hereafter we take  $J$  as the unit of energy. We

also take the lattice constant to be unity throughout this paper.

We investigate the quench dynamic starting from the disordered state  $|\psi_0\rangle = \otimes_i |-\rangle_i$  at  $\Gamma \rightarrow \infty$  to the disordered parameter region  $\Gamma \in (\Gamma_c, \infty)$ . We study the equal-time longitudinal and connected transverse correlation functions at distance  $\mathbf{r}$ , which are defined as

$$C^{zz}(\mathbf{r}, t) = \langle \psi(t) | \hat{S}_{\mathbf{r}}^z \hat{S}_{\mathbf{0}}^z | \psi(t) \rangle, \quad (2)$$

$$C_{\text{connected}}^{xx}(\mathbf{r}, t) = \langle \psi(t) | \hat{S}_{\mathbf{r}}^x \hat{S}_{\mathbf{0}}^x | \psi(t) \rangle - \langle \psi(t) | \hat{S}_{\mathbf{r}}^x | \psi(t) \rangle \langle \psi(t) | \hat{S}_{\mathbf{0}}^x | \psi(t) \rangle \quad (3)$$

with  $|\psi(t)\rangle = e^{-i\hat{H}t}|\psi_0\rangle$ , respectively. Hereafter, we take the lattice spacing to be unity ( $a = 1$ ). In 1D, we obtain them by the exact calculations via the Jordan-Wigner transformation and by the LSWA via the Holstein-Primakoff transformation. In 2D, we use the tensor-network method, the exact diagonalization (ED) method, and the LSWA. We will summarize each method below.

We extract the group velocity from the envelope of the wave packet in the spin-spin correlation functions. Let us first discuss how the correlation spreading is related to the Lieb-Robinson bound. In a system with short-range interaction, a commutator of any operators  $\hat{O}_A$  and  $\hat{O}_B$  in regions A and B satisfies the relation

$$\|[\hat{O}_A(t), \hat{O}_B]\| \leq \text{const.} \times \exp\left(-\frac{L-vt}{\chi}\right), \quad (4)$$

where  $\hat{O}_A(t) = \exp(i\hat{H}t)\hat{O}_A\exp(-i\hat{H}t)$ ,  $L$  is the distance between the regions A and B, and  $\chi$  is constant [21, 22]. The velocity  $v$  corresponds to the Lieb-Robinson bound. This relation means that the information from the region A is transmitted to the region B up to a time  $t \approx L/v$ . Then, the inequality of the Lieb-Robinson bound ensures that, for any operators  $\hat{O}_A$  and  $\hat{O}_B$  in regions A and B having the distance  $L$ , the expectation value for a state  $|\psi\rangle$  with a finite correlation length  $\chi$  satisfies [49]

$$\begin{aligned} & |\langle \psi(t) | \hat{O}_A \hat{O}_B | \psi(t) \rangle - \langle \psi(t) | \hat{O}_A | \psi(t) \rangle \langle \psi(t) | \hat{O}_B | \psi(t) \rangle| \\ & \leq \text{const.} \times e^{-\frac{L-2vt}{\chi'}}, \end{aligned} \quad (5)$$

where  $\chi'$  is a constant that depends on  $\chi$ . This velocity  $2v$  on the right-hand side corresponds to twice the Lieb-Robinson bound. When the correlation spreading is well described by the quasiparticle, the group velocity ( $v^{\text{group}}$ ) of the fastest quasiparticle is often regarded as the Lieb-Robinson bound [50–53].

To estimate the group velocity of the fastest quasiparticle, we calculate the slope obtained from the peak-time dependence of the distance. In general, the maximum group velocity is larger than the velocity associated with the largest correlation peak location, and they do not have to be the same. On the other hand, the latter value is easy to extract and is often regarded as the maximum

group velocity (particularly in experiments). They do coincide for the quench dynamics in the 1D transverse-field Ising model, as we will see later. Therefore, we regard the velocity associated with the largest correlation peak location as the maximum group velocity and, hereafter, call it the Lieb-Robinson velocity. To avoid confusion, we will use the term ‘‘Lieb-Robinson bound’’ to refer to the actual bound in the inequality and the term ‘‘Lieb-Robinson velocity’’ to refer to the velocity extracted from peak positions. The Lieb-Robinson bound is larger than or equal to the Lieb-Robinson velocity.

Under these circumstances, the Lieb-Robinson velocity gives twice the group velocity ( $2v^{\text{group}}$ ) of a fastest quasiparticle. Intuitively, the factor two originates from pairs of quasiparticles moving to the left or right from a given point. This quasiparticle picture has been discussed intensively in the dynamics of the Bose-Hubbard model [51, 54–56]. In the present analysis, we have presented the group velocity  $v^{\text{group}}$  of a certain single quasiparticle estimated from one half of the slope obtained from the peak-time dependence of the distance.

### A. Exact calculations in 1D

The analytical form of the time-dependent correlation functions can be obtained rigorously for the 1D transverse-field Ising model [46, 57–62]. We briefly review the detailed derivation of the time-dependent correlation functions in Appendix A and present the final results below.

The longitudinal correlation function is represented as a Pfaffian of a  $2r \times 2r$  skew symmetric matrix:

$$C^{zz}(r, t) = (-1)^{\frac{r(r-1)}{2}} \cdot \frac{1}{4} \text{pf} \begin{pmatrix} S & G \\ -G^T & Q \end{pmatrix}. \quad (6)$$

Here elements of the matrices  $S$ ,  $Q$ , and  $G$  are defined as

$$s_{i,j} = \begin{cases} S_{i-1,j-1} & \text{if } i < j \\ -S_{j-1,i-1} & \text{if } i > j \\ 0 & \text{if } i = j \end{cases}, \quad (7)$$

$$q_{i,j} = \begin{cases} Q_{i-1,j-1} & \text{if } i < j \\ -Q_{j-1,i-1} & \text{if } i > j \\ 0 & \text{if } i = j \end{cases}, \quad (8)$$

$$g_{i,j} = G_{i-1,j}, \quad (9)$$

where the time-dependent correlation functions  $S_{i,j}$ ,  $Q_{i,j}$ , and  $G_{i,j}$  are given as

$$S_{i,j} = -\frac{2}{L} \sum_{k>0} \left\{ \cos[k(r_i - r_j)] [|\tilde{u}_k(t)|^2 + |\tilde{v}_k(t)|^2] - i \sin[k(r_i - r_j)] [\tilde{u}_k(t)\tilde{v}_k^*(t) + \tilde{v}_k(t)\tilde{u}_k^*(t)] \right\}, \quad (10)$$

$$Q_{i,j} = +\frac{2}{L} \sum_{k>0} \left\{ \cos[k(r_i - r_j)] [|\tilde{u}_k(t)|^2 + |\tilde{v}_k(t)|^2] + i \sin[k(r_i - r_j)] [\tilde{u}_k(t)\tilde{v}_k^*(t) + \tilde{v}_k(t)\tilde{u}_k^*(t)] \right\}, \quad (11)$$

$$G_{i,j} = -\frac{2}{L} \sum_{k>0} \left\{ \cos[-k(r_i - r_j)] [|\tilde{u}_k(t)|^2 - |\tilde{v}_k(t)|^2] - i \sin[-k(r_i - r_j)] [\tilde{u}_k(t)\tilde{v}_k^*(t) - \tilde{v}_k(t)\tilde{u}_k^*(t)] \right\}. \quad (12)$$

The symbol  $\sum_{k>0}$  means the sum taken over all  $k = 2\pi n/L$  with  $n = 1/2, 3/2, \dots, (L-3)/2, (L-1)/2$  for even  $L$ . For the quench starting from the disordered state ( $\Gamma \rightarrow \infty$ ), the parameters  $\tilde{u}_k(t)$  and  $\tilde{v}_k(t)$  for  $0 < k < \pi$  are described as

$$\tilde{u}_k(t) = i \frac{\tilde{b}'_k}{\omega'_k} \sin \left( 2\omega'_k \times \frac{tJ}{4} \right), \quad (13)$$

$$\tilde{v}_k(t) = -i \cos \left( 2\omega'_k \times \frac{tJ}{4} \right) - \frac{\tilde{a}'_k}{\omega'_k} \sin \left( 2\omega'_k \times \frac{tJ}{4} \right) \quad (14)$$

with

$$\tilde{a}'_k = \frac{2\Gamma}{J} + \cos k, \quad (15)$$

$$\tilde{b}'_k = \sin k, \quad (16)$$

$$\omega'_k = \sqrt{\frac{4\Gamma^2}{J^2} + \frac{4\Gamma}{J} \cos k + 1}, \quad (17)$$

respectively. Parameters with prime symbols indicate physical quantities after the quench. On the other hand, the transverse correlation function is given as

$$C_{\text{connected}}^{xx}(r, t) = -\frac{1}{4} (Q_{0,r} S_{0,r} + G_{r,0} G_{0,r}). \quad (18)$$

We numerically evaluate each correlation function for sufficiently large systems. We use the library for Pfaffian computations [63] in the case of the longitudinal correlation function.

### B. Spin-wave approximation

We investigate a small quench starting from the completely disordered point ( $\Gamma \rightarrow \infty$ ) to the parameter within a disordered phase ( $\Gamma_c^{\text{classical}} \ll \Gamma < \infty$ , where  $\Gamma_c^{\text{classical}} = JD$  with  $D$  being the spatial dimension). We focus on small quantum fluctuations around the disordered state and map quantum Ising spins to bosons using the linearized Holstein-Primakoff transformation [64–68]. The equal-time correlation functions for quantum spins can be obtained by calculating those for bosons. They serve as a good approximation as long as the transverse magnetization is large enough ( $\langle S_i^x \rangle \approx 1/2$ ). We give the detailed derivation in Appendix B and show the obtained spin-spin correlation functions below.

The longitudinal correlation function at distance  $\mathbf{r}$  ( $1 \leq r_\nu \leq L/2$  with  $\nu = 1, 2, \dots, D$ ) is given as

$$C^{zz}(\mathbf{r}, t) = \frac{S}{2L^D} \sum_{\mathbf{k}} e^{i\mathbf{k} \cdot \mathbf{r}} \frac{B'_{\mathbf{k}}}{A'_{\mathbf{k}} + B'_{\mathbf{k}}} (\cos 2\Omega'_{\mathbf{k}} t - 1), \quad (19)$$

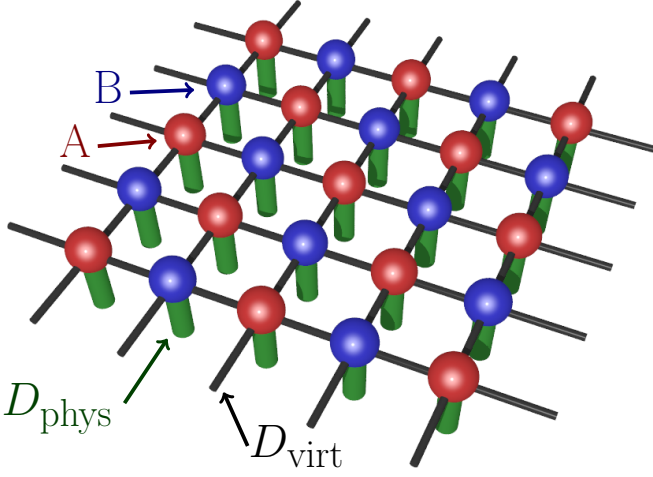


FIG. 1. Schematic picture of the iPEPS having a two-site unit-cell structure. The two sublattice sites are represented by A and B. Each ball corresponds to a rank-five tensor, which is located at a lattice site and has four thin sticks and a thick stick. The thin and thick sticks represent the virtual and physical degrees of freedom, and the bond dimensions of the former and the latter are defined as  $D_{\text{virt}}$  and  $D_{\text{phys}}$ , respectively.

where  $S(=1/2)$  is the size of spin and other parameters are defined as

$$\Omega'_k = \text{sgn}(A'_k) \sqrt{A'_k{}^2 - B'_k{}^2}, \quad (20)$$

$$A'_k = -\frac{z}{2} JS \gamma_k + \Gamma, \quad (21)$$

$$B'_k = -\frac{z}{2} JS \gamma_k, \quad (22)$$

$$\gamma_k = \frac{1}{D} \sum_{\nu=1}^D \cos k_\nu \quad (23)$$

with  $z = 2D$  being the coordination number. Parameters with prime symbols correspond to physical quantities after the quench. On the other hand, the transverse correlation function at distance  $\mathbf{r}$  ( $1 \leq r_\nu \leq L/2$  with  $\nu = 1, 2, \dots, D$ ) is given as

$$\begin{aligned} & C_{\text{connected}}^{xx}(\mathbf{r}, t) \\ &= \left| \frac{1}{L^D} \sum_{\mathbf{k}} e^{i\mathbf{k}\cdot\mathbf{r}} \frac{B'_k}{2\Omega'_k} \left[ \frac{A'_k}{\Omega'_k} (\cos 2\Omega'_k t - 1) + i \sin 2\Omega'_k t \right] \right|^2 \\ &+ \left| \frac{1}{L^D} \sum_{\mathbf{k}} e^{i\mathbf{k}\cdot\mathbf{r}} \frac{B'_k{}^2}{2\Omega'_k{}^2} (\cos 2\Omega'_k t - 1) \right|^2. \end{aligned} \quad (24)$$

We numerically calculate each correlation function for sufficiently large systems.

### C. 2D tensor-network method

We use the infinite projected entangled pair state (iPEPS) [69–76] or the infinite tensor product state [77–

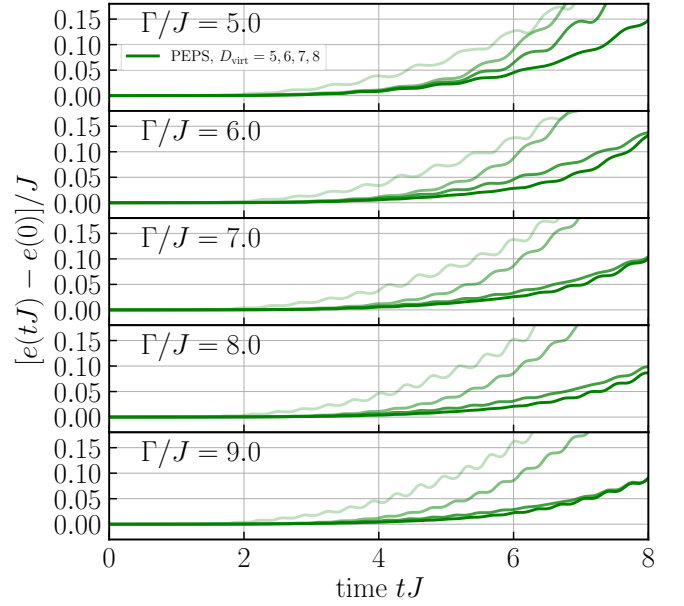


FIG. 2. Bond-dimension dependence of energy density obtained by iPEPS simulations. We consider the quench to  $\Gamma/J = 5, 6, 7, 8,$  and  $9$  and subtract the energy density at  $t = 0$ . The lines correspond to the time-dependent energy density for the bond dimensions  $D_{\text{virt}} = 5, 6, 7,$  and  $8$  (from lighter to darker). The energy is nearly conserved for  $D_{\text{virt}} \geq 6$  in a time frame  $tJ \in [0, 4]$ .

[81] to investigate short-time dynamics in the infinite system. We choose translationally invariant iPEPS consisting of a two-site unit-cell structure as shown in Fig. 1. The dimension of the local Hilbert space is  $D_{\text{phys}} = 2$  for spin  $S = 1/2$ . The initial state  $|\psi_0\rangle = \otimes_i |\rightarrow\rangle_i$  is the ground state in the limit of  $\Gamma/J \rightarrow \infty$ , which can be prepared by the virtual bond dimension  $D_{\text{virt}} = 1$ .

We apply the simple update algorithm [73, 82] to simulate the real-time dynamics of the transverse-field Ising model. In this algorithm, we approximate the real-time evolution operator in a very short-time step  $dt$  using the Suzuki-Trotter decomposition [83–85] and obtain the two-site gate  $e^{-idt\hat{H}} \approx \prod_{(i,j)} e^{-idt\hat{H}_{ij}}$  with  $\hat{H}_{ij} = -J\hat{S}_i^z\hat{S}_j^z - \Gamma(\hat{S}_i^x + \hat{S}_j^x)/z$  ( $z = 4$ ) satisfying  $\hat{H} = \sum_{(i,j)} \hat{H}_{ij}$ . The gate acts on two neighboring tensors and increases the virtual bond dimensions. We truncate the bond dimensions of the local tensors using the singular value decomposition so that the bond dimensions of iPEPS remains  $D_{\text{virt}}$ . Note that the decomposition temporarily breaks the one-site translation symmetry into a two-site one and calls for at least a two-site unit-cell structure even when the system is translation invariant [73, 82]. In the actual calculations, the second-order Suzuki-Trotter decomposition is used, and the time step is typically chosen as  $dtJ = 0.001$  for a quench to a strong field  $\Gamma$ . Simulations using doubled or halved  $dt$  show no significant change in the short-time dynamics as for the present model.

We improve the accuracy of time-evolved wave functions by increasing the dimension of the virtual bond  $D_{\text{virt}}$  and confirm the convergence of physical quantities. Previous studies [41, 43] suggest that results for bond dimensions  $D_{\text{virt}} \gtrsim 6$  already show good convergence within a short-time frame  $tJ \lesssim 4$  even in one of the most difficult cases, i.e., the quench to the critical point. (Concerning the unit of time, the energy scale is four times larger in previous studies [41, 43] because they used the Pauli spin  $\sigma^z = 2S^z$ .)

In the present iPEPS simulations, we adopt the tensor-network library TeNeS [86–88] and increase the virtual bond dimensions up to  $D_{\text{virt}} = 8$  for safety. In general, as for numerical simulations of a quench dynamics, the obtained correlations would be reliable in a short time that the energy is conserved. We investigate the time dependence of the energy density in the unit of Ising interaction  $J$  for different fields  $\Gamma/J$  with increasing the bond dimensions  $D_{\text{virt}}$  (see Fig. 2). The energy density is nearly conserved for a short time ( $tJ \lesssim 4$ ) when  $D_{\text{virt}} \geq 6$  regardless of the choice of the transverse field.

The corner transfer matrix renormalization group method [74–76, 78, 89–95] is used to calculate physical quantities in the thermodynamic limit. We take the bond dimensions of the environment tensors as  $\chi_{\text{virt}} = 2(D_{\text{virt}})^2$  so that physical quantities are well converged.

#### D. Exact diagonalization method

The ED method is often used to get insight into the dynamics of small quantum many-body systems [96–100]. We use the QuSpin library [101, 102] for ED calculations. We consider the system sizes up to 28 sites under the periodic boundary condition. In the present setup, both the Hamiltonian and the initial state are translationally invariant, and the total momentum of the initial and time-evolved states remains zero. We restrict ourselves to the zero-momentum sector [103] and follow the dynamics of the state. Instead of generating matrix elements on the fly to reduce the memory cost, we keep all the elements of sparse matrices in the compressed sparse row format to accelerate calculations. To compute the matrix exponential applied to a vector, we use the Taylor series expansion with error analysis proposed by Al-Mohy and Higham [104, 105].

We confirm that the ED results (up to 28 sites) reproduce the exact analytical results in 1D (not shown). We mainly show the ED results in 2D (for  $5 \times 5$  sites) hereafter.

### III. RESULTS IN 1D

We first present the time dependence of spin-spin correlations in 1D using the exact analytical approach and the LSWA. We extract the group velocity after a sudden quench to a strong field from these data.

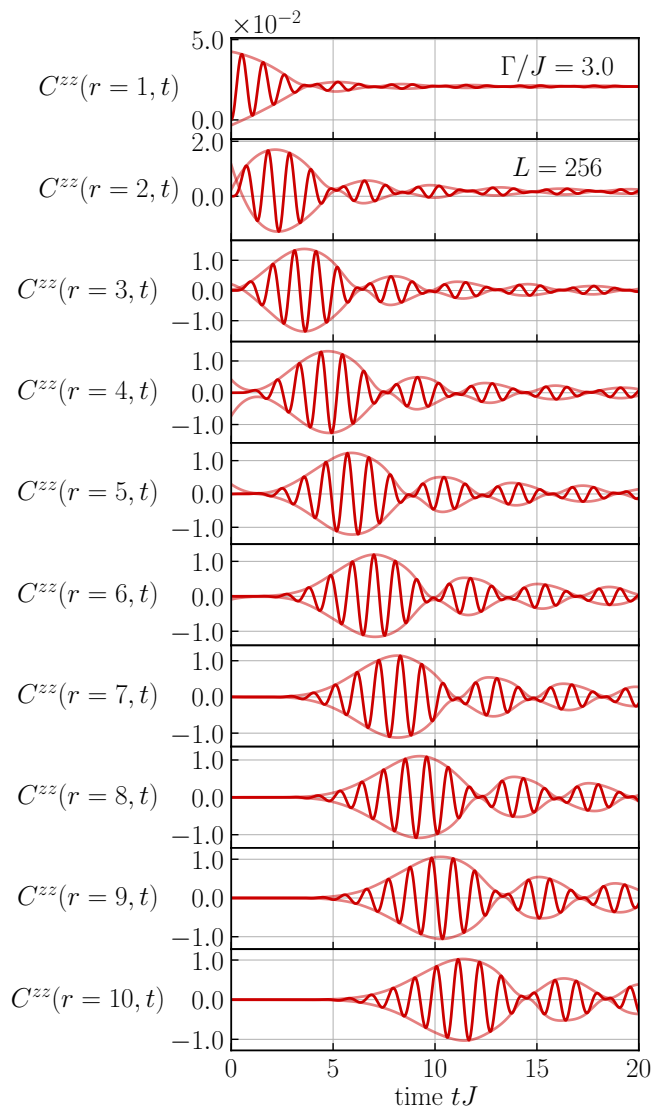


FIG. 3. Exact equal-time longitudinal correlation functions in 1D. We consider the quench to  $\Gamma/J = 3$  for a system size  $L = 256$  and show the short-time dynamics for distances  $r = 1, 2, \dots$ , and 10. The envelope of each correlation function is a guide to the eye. The upper (lower) part of the envelope at each distance is obtained by first searching all the local maxima (minima) in the correlation and then interpolating them using a one-dimensional cubic B-spline curve [106].

#### A. Exact results

We show the exact equal-time longitudinal correlation functions in Fig. 3. At an early time ( $tJ \ll r$ ), the intensity of correlation is nearly zero. On the other hand, when  $tJ \gtrsim r$ , the correlation starts to develop and exhibits rapid oscillations. For each distance, the earliest peak in the envelope of the wave packet has the largest intensity. The peak time of the largest envelope peak moves almost linearly with the distance, suggesting the light-cone-like spreading of correlations.

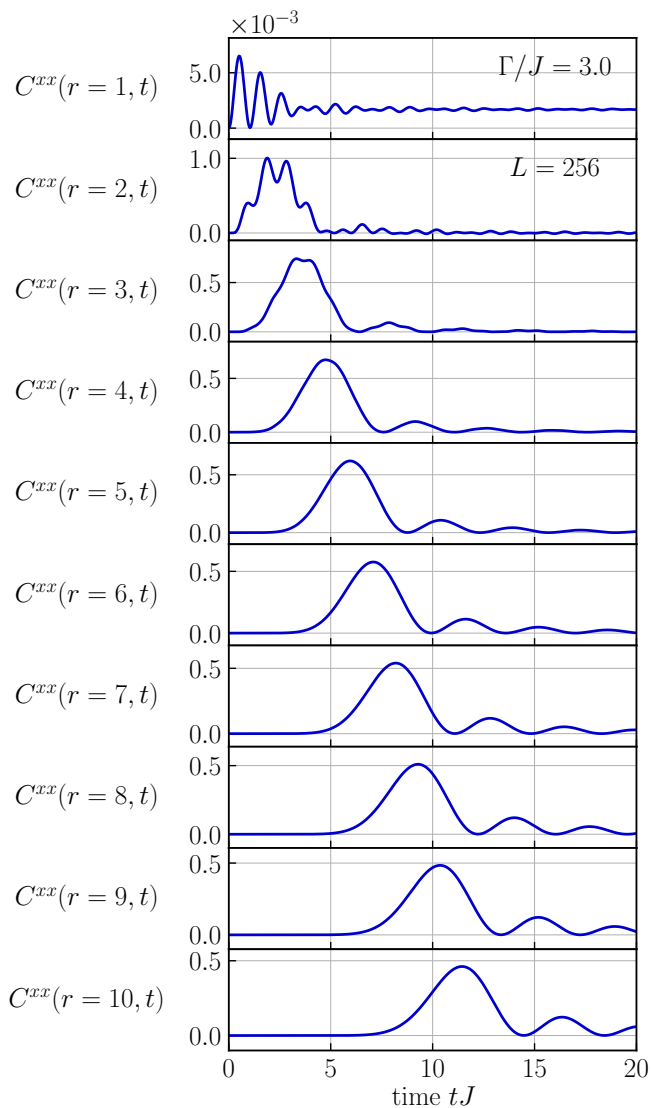


FIG. 4. Exact equal-time transverse correlation functions in 1D. The parameters are the same as those in Fig. 3.

We also show the exact equal-time transverse correlation functions in Fig. 4. In contrast to the longitudinal correlations, the rapid oscillations appear only for short distances ( $r \lesssim 3$ ) and are negligibly small for most of the distances. Besides, the intensity of the transverse correlation is much smaller than that of the longitudinal one. On the other hand, the peak time of the transverse correlation almost coincides with that of the largest envelope peak in the longitudinal correlation. The transverse correlation decays rapidly just before and after the peak time.

To estimate the propagation velocity, we first extract the peak time of the envelope of correlations as a function of distance. We show the corresponding time and distance in Fig. 5. The data for longitudinal and transverse correlations overlap very well. The distance is nearly proportional to the peak time for both correlations. For

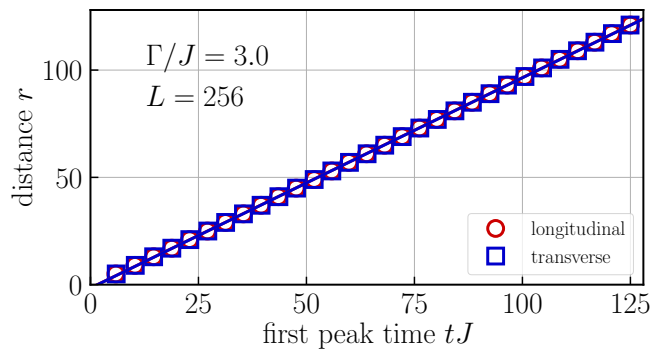


FIG. 5. First-peak time dependence of distance for exact correlations in 1D. We show data points when the distance is a multiple of four. The group velocity is estimated from one half of the slope.

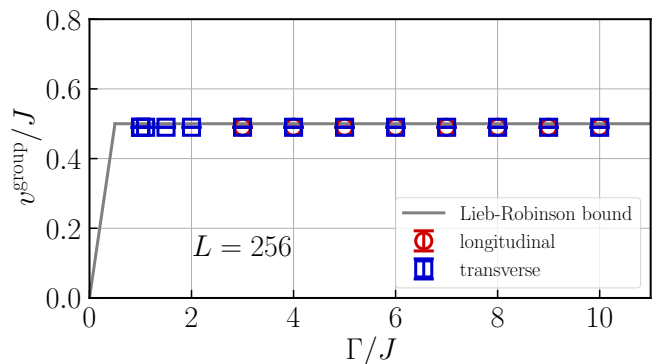


FIG. 6. Field dependence of the group velocity in 1D. The exact Lieb-Robinson velocity  $v^{\text{LR}}/J = 1/2$  is shown as a reference. For  $\Gamma/J < 3$ , we only show the group velocity estimated from the transverse correlations because the envelopes of longitudinal correlations become unclear for a weaker field.

each field  $\Gamma/J$  and size  $L$ , we estimate the group velocity  $v^{\text{group}}$  from one half of the slope so that it corresponds directly to the speed of one of quasiparticle pairs moving to the left or right. Since the data points are slightly out of the straight line at the very short and long distances, we discard those for  $r \leq 5$  and  $r \geq L/2 - 5$  when extracting the velocity.

To see how the group velocity behaves as a function of the transverse field, we first examine a sufficiently large system ( $L = 256$ ) as shown in Fig. 6. Both velocities estimated from longitudinal and transverse correlations are nearly  $0.5J$  for all fields  $\Gamma/J \geq 3$ . The group velocity of the spin-spin correlations agrees with the exact Lieb-Robinson velocity in the 1D transverse-field Ising model (see Appendix A 5 for the derivation of the exact value). This fact suggests that the quasiparticles with the fastest propagation velocity among the various correlation functions are directly responsible for the spreading of spin-spin correlations.

Although the estimated velocity is very close to  $0.5J$ , it is slightly smaller than the exact value in finite-size

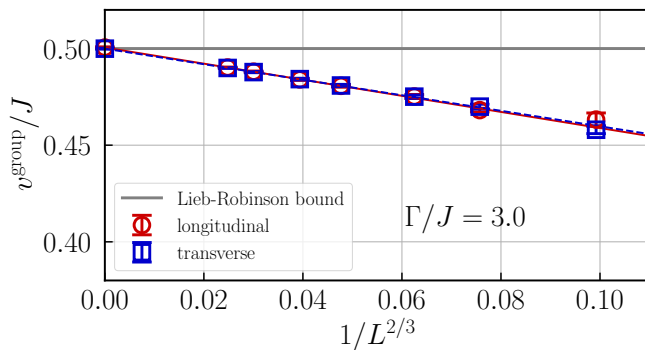


FIG. 7. Size scaling of the group velocity in 1D. The group velocity is well fitted by  $1/L^{2/3}$  with  $L$  being the length of a chain and is extrapolated to the value of the exact Lieb-Robinson velocity  $v^{\text{LR}}/J = 1/2$ .

systems. To check the size dependence and confirm the convergence, we perform the finite-size scaling of the estimated velocity.

For this purpose, let us first discuss how the finite-size effect appears. The spin-spin correlation functions in the 1D transverse-field Ising model are described by the single-particle correlation functions of fermionic quasiparticles. In the thermodynamic limit, they are given by the Bessel functions [59]. The size dependence of the Bessel functions has been carefully investigated in the case of long-time dynamics of the 1D Bose-Hubbard model [54], as well as in that of the 1D transverse-field Ising model [107]. The distance  $r$  dependence of the peak time  $t$  is given as

$$t \approx \frac{1}{v_{\infty}}(r + \epsilon r^{1/3}), \quad (25)$$

where  $v_{\infty}$  is the velocity at large distances, and  $\epsilon$  is a constant related to the peak position of the Bessel function [54]. The instantaneous velocity  $v(r) = [t(r+1) - t(r)]^{-1}$  at each time  $t$  is independent of distances and becomes  $v_{\infty}$  if  $\epsilon = 0$ , but it is slightly modified in the presence of finite  $\epsilon$ . For  $\epsilon \neq 0$ , the instantaneous velocity is obtained as

$$v(r) \approx v_{\infty} \left(1 - \frac{\epsilon}{3} r^{-2/3}\right). \quad (26)$$

Since the farthest distance for a chain of length  $L$  is  $r = L/2$  ( $\propto L$ ), we may safely assume that the deviation between the finite-size and infinite-size velocities  $\Delta v(L)$  follows the relation

$$\Delta v(L) := \left| v\left(\frac{L}{2}\right) - \lim_{L \rightarrow \infty} v\left(\frac{L}{2}\right) \right| \propto L^{-2/3} \quad (27)$$

for  $L \gg 1$ .

We then extrapolate the finite-size group velocities to the thermodynamic limit using Eq. (27). We estimate the error bars using the covariance obtained from weighted least squares regression. As shown in Fig. 7, all the data

points lie on an expected straight line for both correlations. The extrapolated group velocity at  $\Gamma/J = 3$  is  $v^{\text{group}}/J = 0.5005(4)$  [ $v^{\text{group}}/J = 0.4999(3)$ ] for the longitudinal (transverse) correlations and almost converges to the exact Lieb-Robinson velocity ( $v^{\text{LR}}/J = 0.5$ ) of the 1D transverse field Ising model within the error bar of the extrapolation. We have also confirmed that the estimated velocity converges to the exact one for all the other transverse fields that we have studied ( $\Gamma/J \geq 1$ ). Therefore, the fastest correlation spreading can be measured by the spin-spin correlations in the 1D transverse-field Ising model.

## B. Results by the LSWA

To examine how good the LSWA is as for the correlation spreading, we calculate the equal-time spin-spin correlation functions by the LSWA and compare the results with those of the exact analysis. In general, the LSWA gets better with increasing spatial dimensions [108–110] because it takes into account a correction to the leading order of the mean-field approximation. Here we will demonstrate that the group velocity of the correlation propagation obtained by the LSWA agrees well with the exact one even in the lowest 1D.

We show the longitudinal correlation functions in Fig. 8. As in the case of the exact analysis, the correlations are suppressed for  $tJ \lesssim r$  and begin to develop for  $tJ \gtrsim r$  at a given distance  $r$ . The LSWA quantitatively reproduces the period of oscillations and the intensity of exact correlations up to about  $tJ \approx r$ . In the short time ( $tJ \lesssim r$ ), a very small number of quasiparticle excitations would come into play, and the LSWA becomes more accurate in this dilute regime.

On the other hand, the transverse correlation functions appear to be accurate up to the point where they begin to increase (see Fig. 9). In contrast to the exact analytical result, where the earliest peak has the largest intensity, the LSWA predicts that the second earliest peak has the largest intensity. Nevertheless, the time of maximum intensity does not differ significantly between the exact and approximate results. The first-peak time is typically about  $2tJ$  early, while the time of maximum intensity is typically about  $2tJ$  late for all distances in the case of the LSWA. These effects do not change the propagation velocity significantly. Therefore, the group velocity estimated by the LSWA is expected to be close to the exact one.

As in the case of exact analysis, we observe the suppression of rapid oscillations in the transverse correlations using the LSWA. This phenomenon can be easily understood in the magnon picture. The original transverse correlation corresponds to the density-density correlation of magnons. The density operator is less susceptible to the effects of phases. On the other hand, the original longitudinal correlation corresponds to the single-particle correlation of magnons, which directly feels the effects of

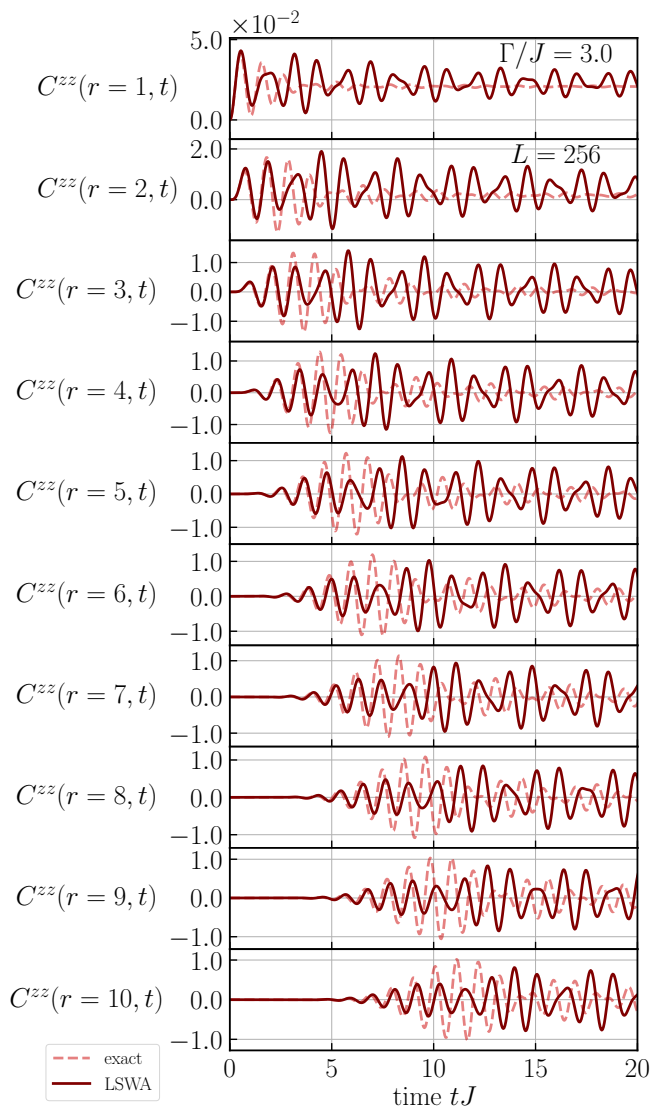


FIG. 8. Equal-time longitudinal correlation functions obtained by the LSWA in 1D. The parameters are the same as those in Fig. 3. We show the exact correlations (dashed line) for comparison.

phases. Therefore, the transverse (longitudinal) correlation tends to exhibit less (more) oscillations. Such effects have been intensively examined in the correlation spreading of the Bose-Hubbard model [51, 54, 55, 111, 112].

Likewise, the LSWA also predicts that the intensity of the transverse correlation is smaller than that of the longitudinal one. They are approximately given as  $|C^{zz}(\mathbf{r}, t)| = \mathcal{O}(J/\Gamma)$  and  $|C_{\text{connected}}^{xx}(\mathbf{r}, t)| = \mathcal{O}(J^2/\Gamma^2)$ , respectively (see Appendices B 2 and B 3).

Having assessed the accuracy of the LSWA, we extract the group velocity from the 1D correlations. We first investigate the distance dependence of peak time for a sufficiently large system ( $L = 256$ ), as shown in Fig. 10. Again, both correlations show almost the same result, and the distance is nearly proportional to the peak time.

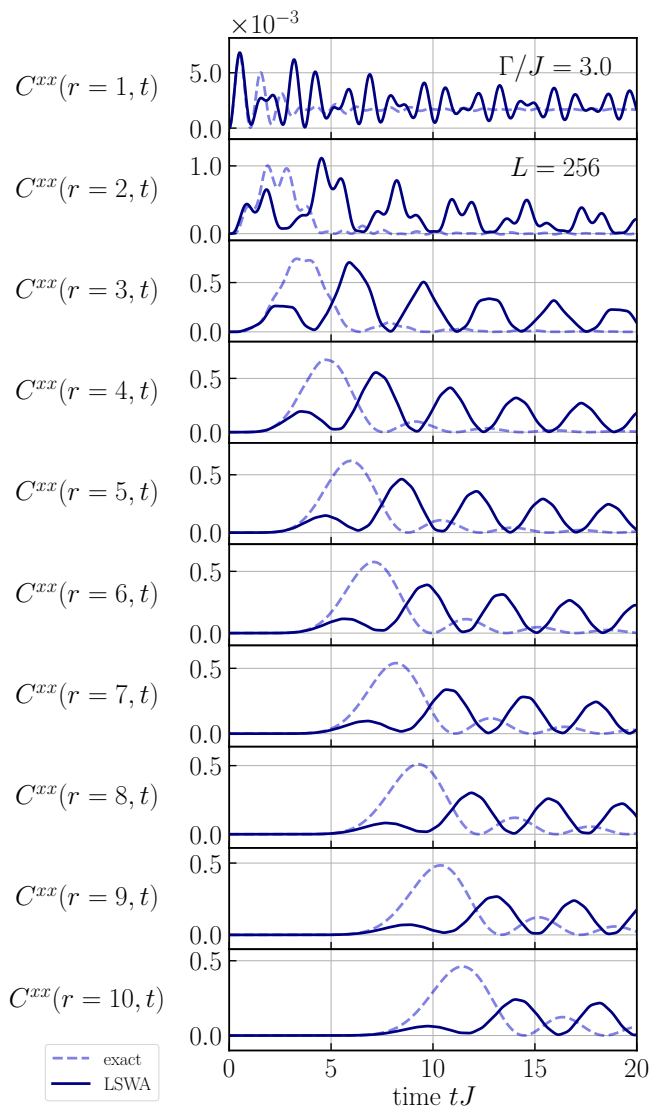


FIG. 9. Equal-time transverse correlation functions obtained by the LSWA in 1D. The parameters are the same as those in Fig. 3. We show the exact correlations (dashed line) for comparison.

We estimate the velocity using the data for  $5 < r < L/2 - 5$ .

We summarize the field dependence of the group velocity in Fig. 11. Both group velocities estimated from the longitudinal and transverse correlations are nearly  $0.5J$  irrespective of the choice of the transverse field for  $\Gamma/J \gtrsim 3$ . Note that the LSWA group velocity is expected to deviate from the exact one at  $\Gamma/J \lesssim 2$  because too many quasiparticles are created due to such a large quench.

Finally, we have confirmed the size dependence of the estimated group velocity. As shown in Fig. 12, the LSWA shows much smaller size dependence than the exact analysis in Fig. 7. The velocity is nearly converged for  $L \geq 48$  and is extrapolated to  $0.5J$ , corresponding to the Lieb-

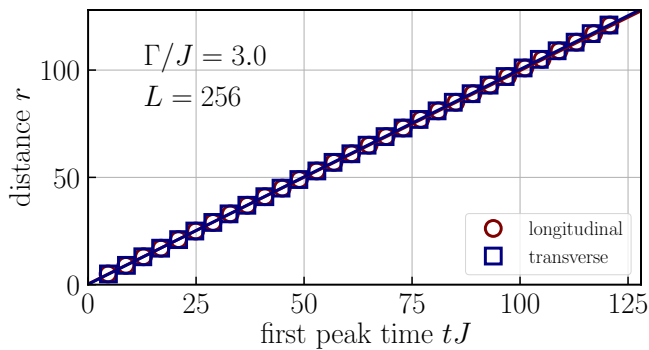


FIG. 10. First-peak time dependence of distance for correlations obtained by the LSWA in 1D. We show data points when the distance is a multiple of four.

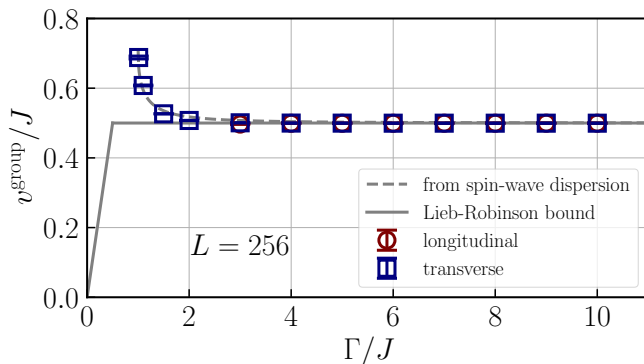


FIG. 11. Field dependence of the group velocity obtained by the LSWA in 1D. The exact Lieb-Robinson velocity  $v^{\text{LR}}/J = 1/2$  and the maximum group velocity  $v^{\text{SW}}/J = [1 + \sqrt{1 - (J/\Gamma)^2}]^{-1/2}/\sqrt{2}$  estimated from the spin-wave dispersion (see Appendix B 4) are shown as references. For  $\Gamma/J < 3$ , we only show the group velocity estimated from the transverse correlations because the envelopes of longitudinal correlations become unclear for a weaker field.

Robinson velocity.

#### IV. RESULTS IN 2D

Next, we examine the time-dependent correlations in 2D using the ED method, the tensor-network method based on iPEPS, and the LSWA. As in the case of 1D, we estimate the group velocity after a sudden quench to a strong field.

##### A. Results by the LSWA

We apply the LSWA to calculate the spin-spin correlation functions and to extract the group velocity. In the case of the 1D transverse-field Ising model, the LSWA reproduces the exact results to the extent that the group velocity of the correlation propagation quan-

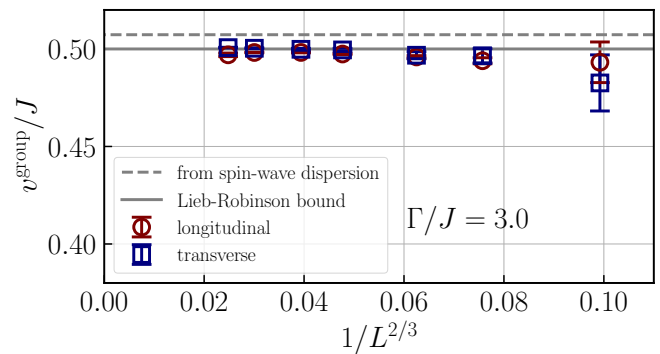


FIG. 12. Size dependence of the group velocity estimated by the LSWA in 1D. The size dependence is smaller than the exact case (see Fig. 7).

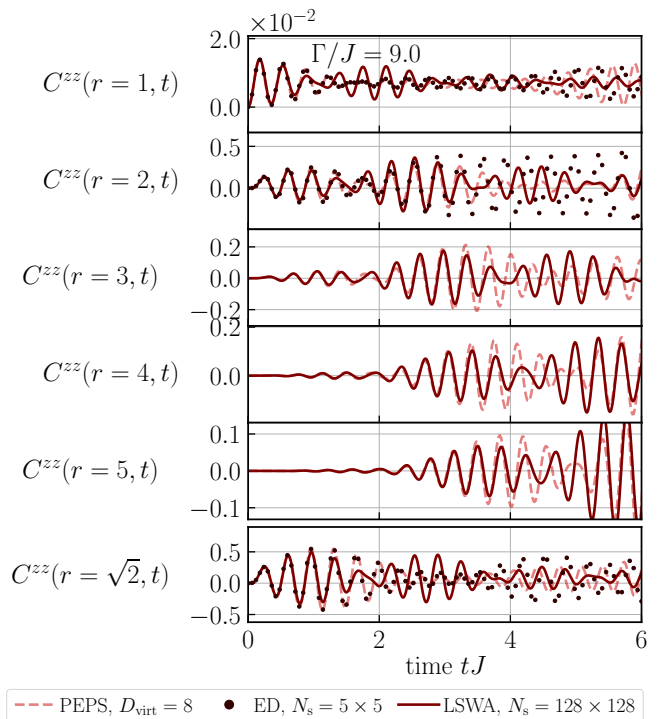


FIG. 13. Equal-time longitudinal correlation functions obtained by the LSWA, the ED method, and the tensor-network method in 2D. We consider the quench to  $\Gamma/J = 9$  for a finite system of  $N_s = L^2$ ,  $L = 128$  by the LSWA (solid line), for a finite system of  $N_s = L^2$ ,  $L = 5$  by ED simulations (small circles), and for the infinite system with the bond dimensions  $D_{\text{virt}} = 8$  by iPEPS simulations (dashed line).

titatively agrees at a sufficiently strong field. We will demonstrate that it reproduces the 2D correlations obtained by the nearly exact simulations much better than in 1D. It also allows us to estimate the group velocity from the correlations at farther distances than the ED and iPEPS simulations, as we will demonstrate below.

We compare the longitudinal correlation functions obtained by the ED method and the LSWA in Fig. 13. The

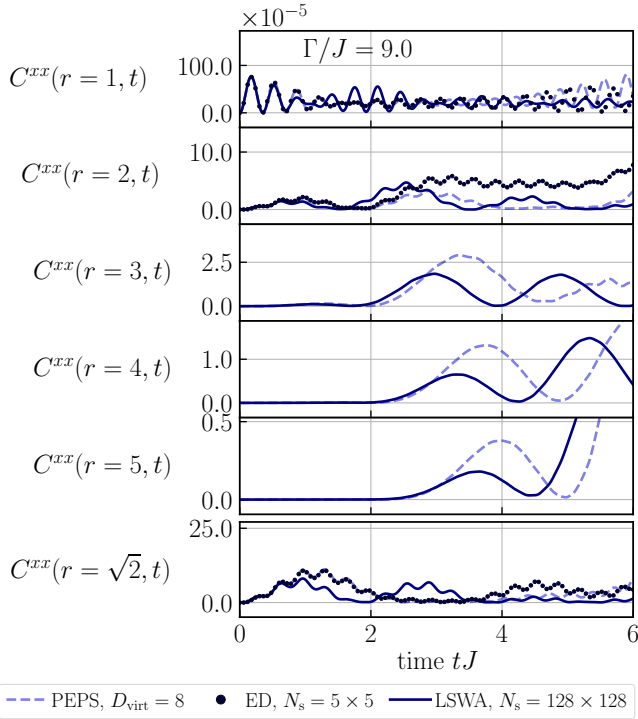


FIG. 14. Equal-time transverse correlation functions obtained by the LSWA, the ED method, and the tensor-network method in 2D. The parameters are the same as those in Fig. 13.

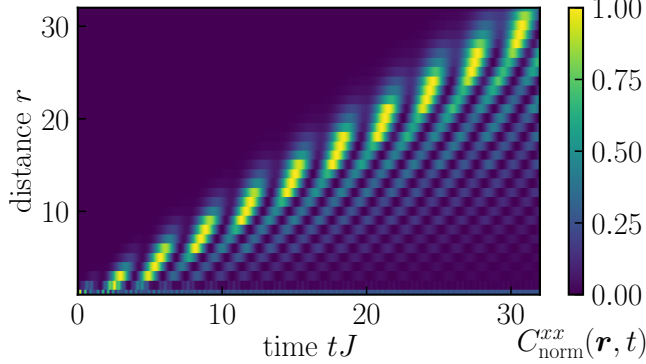


FIG. 15. Contour plot of normalized intensity of equal-time transverse correlation functions as a function of equal-time and distance obtained by the LSWA in 2D. The parameters  $L = 128$  and  $\Gamma/J = 9$  are the same as those in Fig. 13. We show the normalized correlation function  $C_{\text{norm}}^{xx}(\mathbf{r}, t) := C_{\text{connected}}^{xx}(\mathbf{r}, t) / \max_{t \in [0, L/(2J)]} C_{\text{connected}}^{xx}(\mathbf{r}, t) \in [0, 1]$  along the horizontal axis [ $\mathbf{r} = (r, 0)$ ] for each distance up to  $r = 32$ .

LSWA well reproduces the correlations obtained by the ED method up to the point where the second peak of the envelope appears [see, e.g.,  $C^{zz}(r = 2, t)$  in Fig. 13]. The period of oscillations almost coincides between the ED method and the LSWA. As expected in the LSWA in higher spatial dimensions, the agreement in 2D looks much better than in 1D (compare Fig. 8 and Fig. 13).

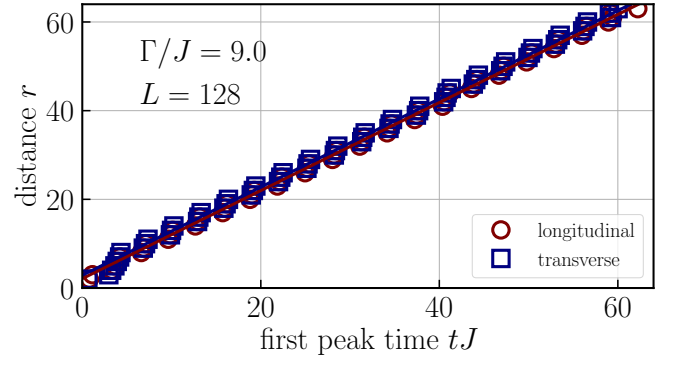


FIG. 16. Dominant-peak time dependence of distance for correlations obtained by the LSWA in 2D.

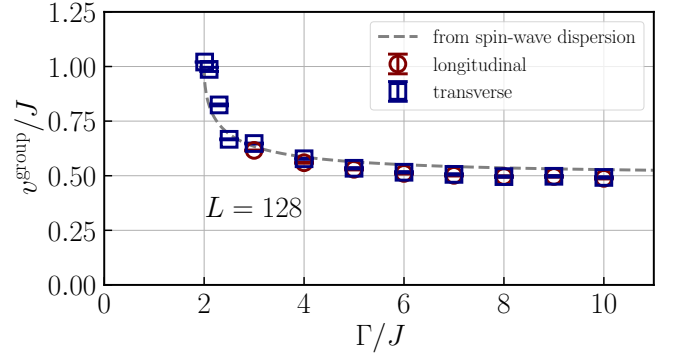


FIG. 17. Field dependence of the group velocity obtained by the LSWA in 2D. The maximum group velocity  $v^{\text{SW}}/J = (1 - J/\Gamma + \sqrt{1 - 2J/\Gamma})^{-1/2}/\sqrt{2}$  estimated from the spin-wave dispersion (see Appendix B 4) is shown as a reference. For  $\Gamma/J < 3$ , we only show the group velocity estimated from the transverse correlations because the envelopes of longitudinal correlations become unclear for a weaker field.

The longitudinal correlations exhibit rapid oscillations as in the case of 1D. On the other hand, in contrast to the 1D case, where the earliest envelope peak has the largest intensity, it does not always exhibit the largest intensity in 2D. The order of the envelope peaks with the largest intensity varies with distance in 2D, which would make it more difficult to extract the group velocity. This observation may be ascribed to the complex interference effects in 2D.

The transverse correlation function obtained by the LSWA also qualitatively reproduces the ED result (see Fig. 14). In contrast to the longitudinal correlations, the rapid oscillations are much weaker for  $r \gtrsim 3$ .

To clarify how the correlation develops for a longer time and to examine the complex interference effects in 2D, we depict the normalized intensity of the transverse correlations as a function of time and distance in Fig. 15. In general, the LSWA performs better in the dilute regime, corresponding to the region  $r \gtrsim tJ$ . Within this range, we observe a stronger intensity near the line satisfying  $r \approx tJ$ . However, areas of high intensity are

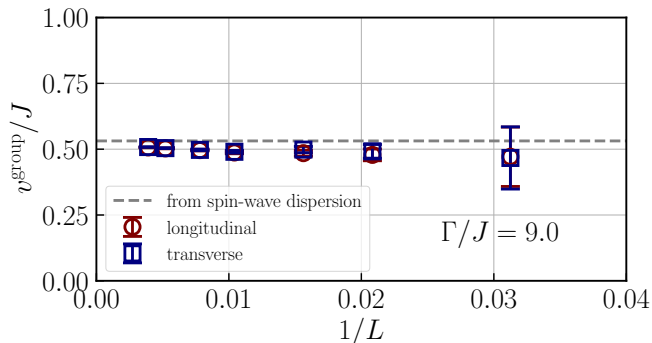


FIG. 18. Size dependence of the group velocity estimated by the LSWA in 2D.

not continuously connected and are rather separated in small pieces. Such pieces are bundled together forming the boundary of the light cone. When we focus on the short-time and short-distance region, we can only look at the first small area of high intensity. If we use such data, we would incorrectly estimate the group velocity. Indeed, as we will see later in Sec. IV B, the velocity obtained by the iPEPS method for a relatively short time has a considerable degree of ambiguity.

To estimate the group velocity in 2D, we collect the peak times and distances in Fig. 16. Both correlations exhibit the consistent results. Although the jagged behavior caused by the complex interference effects is observed in the data points, the distance becomes nearly proportional to the peak time for sufficiently large systems. We extract the group velocity from one half of the slope so that it corresponds directly to the velocity of one quasiparticle.

We show the field dependence of the group velocity along the horizontal axis for a large system ( $N_s = L^2$ ,  $L = 128$ ) in Fig. 17. At a very strong transverse field, the velocity turns out to be nearly  $0.5J$ . The velocity is likely to increase with decreasing the transverse field. This observation is qualitatively consistent with the result obtained in perturbation theory (see Appendix B 4). The velocity estimated from correlations is basically on the curve represented by  $v^{\text{SW}}/J = (1 - J/\Gamma + \sqrt{1 - 2J/\Gamma})^{-1/2}/\sqrt{2}$ , which is determined by the derivative of the spin-wave dispersion (see Appendix B 4).

We finally check the size dependence of the estimated group velocity in Fig. 18. As in the case of 1D, the velocity does not depend on the size significantly for  $L \gtrsim 48$  and converges to the value close to  $0.5J$ . Therefore, the LSWA predicts that the speed of spin-spin correlation spreading is  $v^{\text{group}} \approx 0.5J$  for a small quench to  $\Gamma \gg J$  in the 2D transverse-field Ising model.

## B. Tensor-network results

As a complementary method to the LSWA, we use the tensor-network method based on the iPEPS to calculate

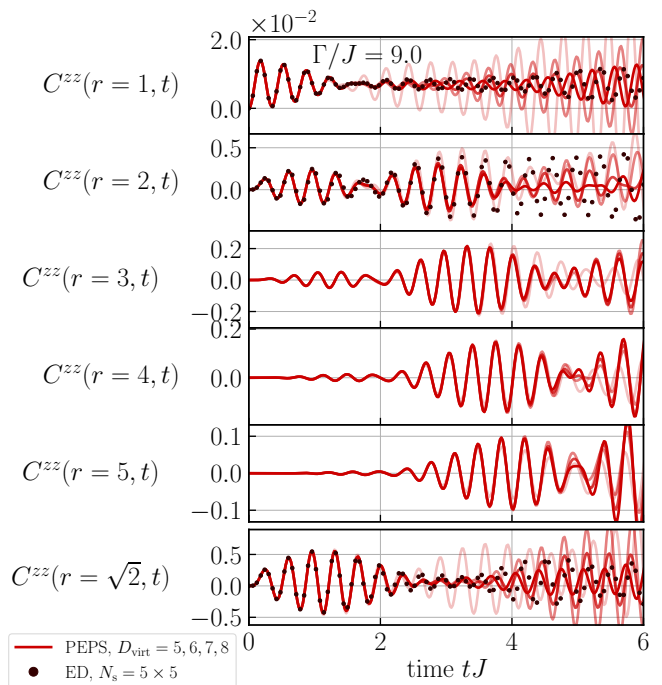


FIG. 19. Equal-time longitudinal correlation functions in 2D. We consider the quench to  $\Gamma/J = 9$  for the infinite system with the bond dimensions  $D_{\text{virt}} = 5, 6, 7, 8$  (solid lines from lighter to darker) by iPEPS simulations and for a finite system of  $N_s = L^2$ ,  $L = 5$  (small circles) by ED simulations. We show the short-time dynamics for distances  $r = 1, 2, \dots, 5$ , and  $\sqrt{2}$ . Both data agree very well for  $t/J \lesssim 4$ .

the spin-spin correlation functions. We will see that the tensor-network method has an advantage in calculating the time dependence of correlations more accurately than the LSWA.

Before presenting the correlations obtained by the iPEPS simulations, let us comment on the time range of the applicability of the method. As we have discussed in Sec. II C, as for numerical simulations of a quench dynamics, the obtained correlations would be reliable in a short time that the energy is conserved. In our case, the energy density is found to be nearly conserved for a short time ( $tJ \lesssim 4$ ) when  $D_{\text{virt}} \geq 6$  (see Fig. 2). Therefore, we will present the correlations within this time frame hereafter.

We show the longitudinal correlation functions obtained by the ED and iPEPS simulations in Fig. 19. The ED method can deal with small systems in 2D and gives the correlations up to  $r \approx 2$  at the farthest. For these distances ( $r \lesssim 2$ ) and short times ( $tJ \lesssim 4$ ), the data by the ED and iPEPS methods completely overlap. Since the iPEPS method directly handles the infinite system, the ED method appears to provide the correlations that can almost be regarded as those at the thermodynamic limit in this regime. The iPEPS method can predict the peak positions of correlations at slightly farther distances and still conserve the energy for  $tJ \lesssim 4$ . The peak in the

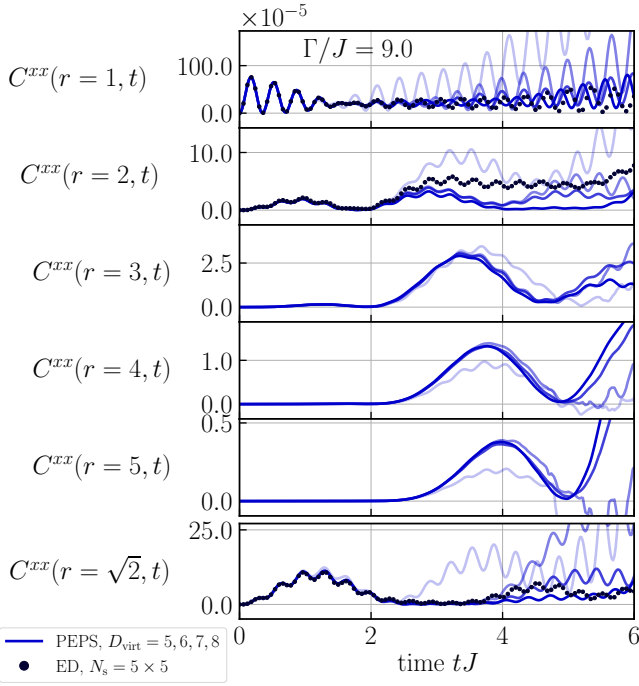


FIG. 20. Equal-time transverse correlation functions in 2D. The parameters are the same as those in Fig. 19.

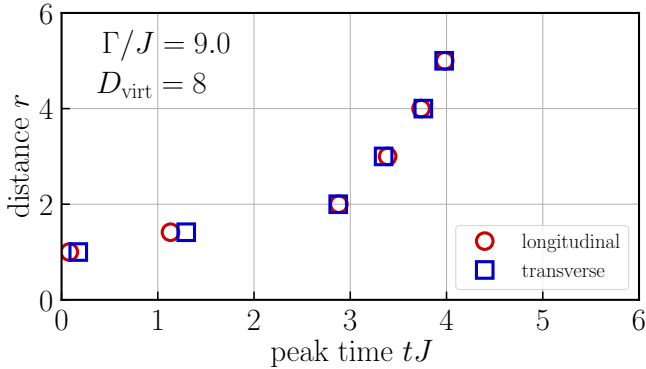


FIG. 21. Dominant-peak time dependence of distance for correlations obtained by iPEPS simulations ( $D_{\text{virt}} = 8$ ) in 2D. The group velocity is estimated from the value  $r/[2t(r)]$  for distances  $r = 3, 4$ , and  $5$ .

envelope of correlation hits  $tJ \approx 4$  when  $r = 5$ , and thus the correlations up to  $r = 5$  would be reliable for the velocity estimation.

As in the case of the LSWA, the longitudinal correlations exhibit rapid oscillations. Moreover, in 2D, the tensor-network method also predicts that the earliest envelope peak does not always correspond to the peak having the largest intensity (see Fig. 19). This observation suggests that the complex interference effects in 2D are not the artifact of the LSWA.

We also examine the transverse correlation functions in Fig. 20. The ED and iPEPS methods provide almost

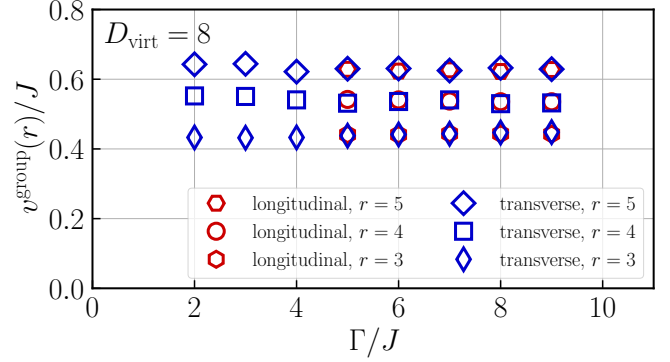


FIG. 22. Field dependence of the group velocity estimated from iPEPS simulations ( $D_{\text{virt}} = 8$ ) in 2D. For  $\Gamma/J < 5$ , we only show the group velocity estimated from the transverse correlations because the envelopes of longitudinal correlations become unclear for a weaker field.

the same correlations for  $r \lesssim 2$  and  $tJ \lesssim 4$ . Again, the iPEPS method is applicable to farther distances up to  $r = 5$ . The rapid oscillations are quickly suppressed for  $r \gtrsim 3$ , as in the case of 1D and also as in the LSWA for 2D. The peak positions of the transverse correlations are nearly the same as those of the envelope peak in the longitudinal correlations.

The qualitative behavior of correlations obtained by the tensor-network method and the LSWA is similar (see Figs. 13 and 14). The peak time of the correlations does not differ significantly between the two methods. Although the first-peak time is a little ahead in the LSWA, the peak-time difference is typically  $0.5tJ$  in 2D, which is smaller than  $2tJ$  in 1D. Because the LSWA is applicable to a much longer time, it is more suitable for estimating the group velocity. On the other hand, the time dependences of correlations agree well between the ED and tensor-network methods, whereas they slightly differ between the ED method and the LSWA. Therefore, the tensor-network method is more appropriate to obtain quantitative data.

To estimate the group velocity, we pick up the peak time for each distance from these correlations obtained by iPEPS simulations, as shown in Fig. 21. Since the data obtained by the bond dimensions  $D_{\text{virt}} = 6, 7$ , and  $8$  are well converged, we present the result for the largest bond dimension  $D_{\text{virt}} = 8$ . Within the range of time where the iPEPS simulations are considered to be reliable, it is hard to tell whether the light-cone-like spreading of correlations exists or not in 2D. However, as we have shown by the LSWA in Sec. IV A, such behavior is caused by the complex interference effects in 2D; it is highly probable that the light cone exists. Therefore, we may assume that the distance eventually grows linearly with the peak time also in the iPEPS results. We then extract the group velocity as  $v^{\text{group}} = r/[2t(r)]$  for each distance  $r$ . We mainly focus on the data for farther distances ( $r = 3, 4$ , and  $5$ ) because data for short distances tend to be off the light-cone behavior in general.

The field dependence of the group velocities along the horizontal axis for distances  $r = 3, 4,$  and  $5$  are given in Fig. 22. They do not vary significantly for  $\Gamma/J \in [2, 9]$ . Since the velocity increases with increasing the distance, we estimate the group velocity as the average of the smallest and largest values with the ambiguity given by one half of their difference. It is given as  $v^{\text{group}}/J \in [0.43, 0.65]$  for all transverse fields that we have studied using the iPEPS method. As we have discussed in Sec. IV A, the LSWA also predicts the similar velocity  $v^{\text{group}}/J \approx 0.5$ . The velocities obtained by the LSWA and those obtained by the tensor-network method agree within the ambiguity.

## V. DISCUSSION AND SUMMARY

Let us compare our group velocity estimated from the spin-spin correlations with the recent Lieb-Robinson bound. In 1D, our estimate of the group velocity is  $v^{\text{group}} = J/2$ . This is the same as the exact Lieb-Robinson velocity  $v^{\text{LR}} = J/2$  in the 1D transverse-field Ising model, indicating that the spin-spin correlations propagate at the speed of fastest quasiparticles. On the other hand, the recent Lieb-Robinson bound for general lattice systems provides the speed  $v^{\text{recent}} = 1.51J$  [23]. As was already pointed out in Ref. [23], it is approximately three times as large as the exact Lieb-Robinson velocity.

In 2D, the group velocity along the horizontal axis is estimated to be  $v^{\text{horizontal}} \approx J/2$  as well. We do not know the exact excitation velocity in the 2D transverse-field Ising model so far. However, for a small quench within a disorder phase, we might expect that the fastest quasiparticles are responsible for spin-correlation spreading also in 2D. We come to this conclusion because the dispersion corresponding to the fastest quasiparticles obtained in perturbation theory [113] turns out to be the same as the dispersion estimated in the LSWA (see Appendix B 4), and the LSWA reproduces the spin-spin correlations obtained by the exact analysis in 1D and those obtained by the nearly exact simulations in 2D fairly well (see Secs. III and IV). Therefore, as for the transverse-field Ising model, even in 2D, it is natural to regard the group velocity of the spin-spin correlations obtained by the LSWA as the Lieb-Robinson velocity. From the comparison between this value (the horizontal  $v^{\text{horizontal}} \approx J/2$  or the diagonal  $v^{\text{diagonal}} \approx J/\sqrt{2}$  velocity) and the best currently available estimate ( $v^{\text{recent, horizontal}} = JX_{y=2} \approx 2.836J$  or  $v^{\text{recent, diagonal}} = 2JX_{y=1/2} \approx 3.787J$ , where  $X_y$  is the solution to the equation  $x \operatorname{arcsinh} x = \sqrt{x^2 + 1} + y$ ) [23], it is likely that there is still much room for improving the Lieb-Robinson bound in 2D.

In conclusion, we have studied the correlation-spreading dynamics in the transverse-field Ising model on a chain and that on a square lattice. We have calculated the longitudinal and transverse spin-spin correla-

tion functions after a sudden quench starting from the disordered state to a strong field within a disordered phase. We have applied several analytical and numerical methods and crossvalidated all data.

In 1D, we have compared the time-dependent correlations using the exact analytical formulae and the LSWA. We have found that the group velocity of the correlation propagation extracted from the LSWA results asymptotically approaches that from the exact analytical formulae as the transverse field increases. In addition, the transverse correlation tends to exhibit less oscillations than the longitudinal one. This fact makes it easier to extract the propagation velocity without drawing the envelope of the wave packet of the correlation when we measure the transverse one. Moreover, the 1D spin-spin correlations are found to propagate at the speed of fastest quasiparticles corresponding to the exact Lieb-Robinson velocity.

In 2D, we have calculated the correlations using the ED method, the tensor-network method based on iPEPS, and the LSWA. As in the case of 1D, we have confirmed that the three methods reproduce nearly the same correlations within a short-time frame. The tensor-network method and the LSWA allow us to calculate the correlations for much farther distances than the ED method can deal with. In particular, the LSWA is convenient for estimating the propagation velocity, whereas the tensor-network method is advantageous in calculating the time dependence of correlations accurately. We have extracted the group velocity by these two methods and obtained the value which is nearly equal to one half of the magnitude of the Ising interaction. The group velocity of the spin-spin correlations in 2D turns out to be much smaller than the best currently available estimate for the Lieb-Robinson bound [23].

Our findings on the group velocity would be helpful for future analog quantum simulations of Rydberg-atom arrays and stimulate further research on the Lieb-Robinson bound. The present tensor-network method, which can accurately calculate the dynamics in one of the most fundamental two-dimensional quantum many-body systems, opens the possibility of future applications to other systems.

## ACKNOWLEDGMENTS

The authors acknowledge fruitful discussions with Shimpei Goto, Daichi Kagamihara, and Mathias Mikkelsen. The authors thank Chen-Yue Guo for correcting typographical errors in equations for the exact longitudinal correlation function in 1D. This work was financially supported by JSPS KAKENHI (Grants Nos. JP18H05228, JP21H01014, and JP21K13855), by MEXT Q-LEAP (Grant No. JPMXS0118069021), and by JST FOREST (Grant No. JPMJFR202T). The numerical computations were performed on computers at the Yukawa Institute Computer Facility and on computers at the Supercomputer Center, the Institute for Solid

State Physics, the University of Tokyo.

## Appendix A: Details of exact calculations in 1D

### 1. Hamiltonian

We review the derivation of the exact form of two-body correlation functions after a sudden quench [46, 57–62]. For simplicity, we consider the Hamiltonian

$$\hat{H} = - \sum_i \hat{\sigma}_i^z \hat{\sigma}_{i+1}^z - \tilde{g} \sum_i \hat{\sigma}_i^x, \quad (\text{A1})$$

which corresponds to the Hamiltonian in Eq. (1) with  $J = 4$  and  $\Gamma = \tilde{g}J/2$ . To get the correlation functions for the original Hamiltonian, we have to use  $\tilde{g} = 2\Gamma/J$  and replace time  $4t$  with  $tJ$ .

After the Jordan-Wigner transformation

$$\hat{\sigma}_i^x = 2\hat{c}_i^\dagger \hat{c}_i - 1, \quad (\text{A2})$$

$$\hat{\sigma}_i^z = \prod_{j=1}^{i-1} (1 - 2\hat{c}_j^\dagger \hat{c}_j) (\hat{c}_i + \hat{c}_i^\dagger) \quad (\text{A3})$$

and the Fourier transformation

$$\hat{c}_j = \frac{1}{\sqrt{L}} \sum_k e^{-ikr_j} \hat{c}_k, \quad (\text{A4})$$

$$k = \frac{2\pi n}{L}, \quad (\text{A5})$$

where  $n = -(L-1)/2, -(L-3)/2, \dots, -1/2, 1/2, \dots, (L-3)/2, (L-1)/2$  for even  $L$  or  $n = -(L-1)/2, (L-3)/2, \dots, -2, -1, 0, 1, 2, \dots, (L-3)/2, (L-1)/2$  for odd  $L$ , we obtain

$$\hat{H} = \sum_k (\hat{c}_k^\dagger \hat{c}_{-k}) \begin{pmatrix} \tilde{a}_k & -i\tilde{b}_k \\ i\tilde{b}_k & -\tilde{a}_k \end{pmatrix} \begin{pmatrix} \hat{c}_k \\ \hat{c}_{-k}^\dagger \end{pmatrix}, \quad (\text{A6})$$

$$\tilde{a}_k = \tilde{g} + \cos k, \quad (\text{A7})$$

$$\tilde{b}_k = \sin k. \quad (\text{A8})$$

Using the Bogoliubov transformation

$$\begin{pmatrix} \hat{c}_k \\ \hat{c}_{-k}^\dagger \end{pmatrix} = \begin{pmatrix} u_k & iv_k \\ iv_k & u_k \end{pmatrix} \begin{pmatrix} \hat{\gamma}_k \\ \hat{\gamma}_{-k}^\dagger \end{pmatrix} \quad (\text{A9})$$

$$u_k = \cos \frac{\theta_k}{2}, \quad (\text{A10})$$

$$v_k = \sin \frac{\theta_k}{2}, \quad (\text{A11})$$

$$\tan \theta_k = \frac{\sin k}{g + \cos k} \quad (\text{A12})$$

satisfying  $u_{-k} = u_k$  and  $v_{-k} = -v_k$ , we get

$$\hat{H} = 2 \sum_k \omega_k \left( \hat{\gamma}_k^\dagger \hat{\gamma}_k - \frac{1}{2} \right), \quad (\text{A13})$$

$$\omega_k = \sqrt{\tilde{g}^2 + 2\tilde{g} \cos k + 1}. \quad (\text{A14})$$

The coefficients  $u_k$  and  $v_k$  can be described by  $\tilde{a}_k, \tilde{b}_k$ , and  $\omega_k$  as

$$u_k = \frac{\tilde{a}_k - \omega_k}{\sqrt{2\omega_k(\omega_k - \tilde{a}_k)}} = \frac{(\tilde{a}_k - \omega_k)\sqrt{\omega_k + \tilde{a}_k}}{\sqrt{2\omega_k}|\tilde{b}_k|}, \quad (\text{A15})$$

$$v_k = \frac{\tilde{b}_k}{\sqrt{2\omega_k(\omega_k - \tilde{a}_k)}} = \frac{\text{sgn}(\tilde{b}_k)\sqrt{\omega_k + \tilde{a}_k}}{\sqrt{2\omega_k}}. \quad (\text{A16})$$

In the present paper, we mainly consider the quantum quench from  $\tilde{g} = g_0$  to  $\tilde{g} = g < \infty$  within the disordered phase. We write the Hamiltonian before (after) the quench as  $\hat{H}$  ( $\hat{H}'$ ). For  $\tilde{g} \rightarrow \infty$ , we have  $u_k \rightarrow 0$  and  $v_k \rightarrow \text{sgn}(\sin k)$ .

### 2. Longitudinal correlation functions

We evaluate the time-dependent longitudinal correlation functions defined as

$$\bar{C}^{zz}(r, t) = \langle \psi_0 | e^{i\hat{H}'t} \hat{\sigma}_i^z \hat{\sigma}_{i+r}^z e^{-i\hat{H}'t} | \psi_0 \rangle \quad (\text{A17})$$

$$= \langle \psi_0 | e^{i\hat{H}'t} (\hat{c}_i^\dagger + \hat{c}_i) \left[ \prod_{j=i}^{i+r-1} (1 - 2\hat{c}_j^\dagger \hat{c}_j) \right] \cdot (\hat{c}_{i+r}^\dagger + \hat{c}_{i+r}) e^{-i\hat{H}'t} | \psi_0 \rangle. \quad (\text{A18})$$

Using the equality  $1 - 2\hat{c}_j^\dagger \hat{c}_j = (\hat{c}_j^\dagger + \hat{c}_j)(\hat{c}_j^\dagger - \hat{c}_j)$  and defining the operators

$$\hat{A}_i = \hat{c}_i^\dagger + \hat{c}_i, \quad \hat{B}_i = \hat{c}_i^\dagger - \hat{c}_i, \quad (\text{A19})$$

$$\hat{A}_i(t) = e^{i\hat{H}'t} \hat{A}_i e^{-i\hat{H}'t}, \quad \hat{B}_i(t) = e^{i\hat{H}'t} \hat{B}_i e^{-i\hat{H}'t}, \quad (\text{A20})$$

we obtain the correlation function

$$\bar{C}^{zz}(r, t) = \langle \psi_0 | \hat{B}_i(t) \hat{A}_{i+1}(t) \hat{B}_{i+1}(t) \hat{A}_{i+2}(t) \hat{B}_{i+2}(t) \cdots \cdot \hat{A}_{i+r-1}(t) \hat{B}_{i+r-1}(t) \hat{A}_{i+r}(t) | \psi_0 \rangle. \quad (\text{A21})$$

It can be evaluated by the Pfaffian of a  $2r \times 2r$  skew symmetric matrix  $A$  using the Wick's theorem:

$$\bar{C}^{zz}(r, t) = (-1)^{\frac{r(r-1)}{2}} \cdot \text{pf} A. \quad (\text{A22})$$

The matrix  $A$  is given as

$$A = \begin{pmatrix} S & G \\ -G^T & Q \end{pmatrix} \quad (\text{A23})$$

with matrices

$$S = \begin{pmatrix} 0 & S_{0,1} & S_{0,2} & \cdots & S_{0,r-2} & S_{0,r-1} \\ -S_{0,1} & 0 & S_{1,2} & \cdots & S_{1,r-2} & S_{1,r-1} \\ -S_{0,2} & -S_{1,2} & 0 & \cdots & S_{2,r-2} & S_{2,r-1} \\ \vdots & \vdots & \vdots & \ddots & \vdots & \vdots \\ -S_{0,r-2} & -S_{1,r-2} & -S_{2,r-2} & \cdots & 0 & S_{r-2,r-1} \\ -S_{0,r-1} & -S_{1,r-1} & -S_{2,r-1} & \cdots & -S_{r-2,r-1} & 0 \end{pmatrix}, \quad (\text{A24})$$

$$Q = \begin{pmatrix} 0 & Q_{0,1} & Q_{0,2} & \cdots & Q_{0,r-2} & Q_{0,r-1} \\ -Q_{0,1} & 0 & Q_{1,2} & \cdots & Q_{1,r-2} & Q_{1,r-1} \\ -Q_{0,2} & -Q_{1,2} & 0 & \cdots & Q_{2,r-2} & Q_{2,r-1} \\ \vdots & \vdots & \vdots & \ddots & \vdots & \vdots \\ -Q_{0,r-2} & -Q_{1,r-2} & -Q_{2,r-2} & \cdots & 0 & Q_{r-2,r-1} \\ -Q_{0,r-1} & -Q_{1,r-1} & -Q_{2,r-1} & \cdots & -Q_{r-2,r-1} & 0 \end{pmatrix}, \quad (\text{A25})$$

$$G = \begin{pmatrix} G_{0,1} & G_{0,2} & G_{0,3} & \cdots & G_{0,r-1} & G_{0,r} \\ G_{1,1} & G_{1,2} & G_{1,3} & \cdots & G_{1,r-1} & G_{1,r} \\ G_{2,1} & G_{2,2} & G_{2,3} & \cdots & G_{2,r-1} & G_{2,r} \\ \vdots & \vdots & \vdots & \ddots & \vdots & \vdots \\ G_{r-2,1} & G_{r-2,2} & G_{r-2,3} & \cdots & G_{r-2,r-1} & G_{r-2,r} \\ G_{r-1,1} & G_{r-1,2} & G_{r-1,3} & \cdots & G_{r-1,r-1} & G_{r-1,r} \end{pmatrix}. \quad (\text{A26})$$

Here we define time-dependent correlation functions

$$S_{i,j} = \langle \hat{B}_i(t) \hat{B}_j(t) \rangle, \quad (\text{A27})$$

$$Q_{i,j} = \langle \hat{A}_i(t) \hat{A}_j(t) \rangle, \quad (\text{A28})$$

$$G_{i,j} = \langle \hat{B}_i(t) \hat{A}_j(t) \rangle = -\langle \hat{A}_j(t) \hat{B}_i(t) \rangle \quad (\text{A29})$$

and use that they are translational invariant. We will obtain the explicit form of evaluating  $S_{i,j}$ ,  $Q_{i,j}$ , and  $G_{i,j}$  in Appendix A 4.

### 3. Transverse correlation functions

We evaluate the time-dependent transverse correlation functions defined as

$$\bar{C}^{xx}(r, t) = \langle \psi_0 | e^{i\hat{H}'t} \hat{\sigma}_i^x \hat{\sigma}_{i+r}^x e^{-i\hat{H}'t} | \psi_0 \rangle \quad (\text{A30})$$

$$= \langle \psi_0 | e^{i\hat{H}'t} (2\hat{c}_i^\dagger \hat{c}_i - 1) (2\hat{c}_{i+r}^\dagger \hat{c}_{i+r} - 1) e^{-i\hat{H}'t} | \psi_0 \rangle. \quad (\text{A31})$$

Using the equality  $1 - 2\hat{c}_j^\dagger \hat{c}_j = (\hat{c}_j^\dagger + \hat{c}_j)(\hat{c}_j^\dagger - \hat{c}_j)$  and the expressions for  $\hat{A}_i$  and  $\hat{B}_i$ , we obtain

$$\bar{C}^{xx}(r, t) = \langle \psi_0 | \hat{A}_i(t) \hat{B}_i(t) \hat{A}_{i+r}(t) \hat{B}_{i+r}(t) | \psi_0 \rangle \quad (\text{A32})$$

$$= G_{i,i}^2 - Q_{i,i+r} S_{i,i+r} + (-G_{i+r,i}) G_{i,i+r}. \quad (\text{A33})$$

Subtracting the correlation of the local transverse magnetization, which is given as  $\langle \hat{\sigma}_i^x(t) \rangle = \langle \psi_0 | e^{i\hat{H}'t} \hat{\sigma}_i^x e^{-i\hat{H}'t} | \psi_0 \rangle = -\langle \psi_0 | \hat{A}_i(t) \hat{B}_i(t) | \psi_0 \rangle = -G_{i,i}$ , we get the connected correlation function

$$\bar{C}_{\text{connected}}^{xx}(r, t) := \bar{C}^{xx}(r, t) - \langle \hat{\sigma}_i^x(t) \rangle \langle \hat{\sigma}_{i+r}^x(t) \rangle \quad (\text{A34})$$

$$= -Q_{i,i+r} S_{i,i+r} - G_{i+r,i} G_{i,i+r}. \quad (\text{A35})$$

The explicit form of evaluating  $S_{i,j}$ ,  $Q_{i,j}$ , and  $G_{i,j}$  will be given in Appendix A 4.

### 4. Single-particle correlation functions for fermions

Let us focus on  $t = 0$  operators. For simplicity, we restrict ourselves to the case of even  $L$ . Using the Fourier

transformation  $\hat{c}_j = \frac{1}{\sqrt{L}} \sum_k e^{-ikrj} \hat{c}_k$  and the Bogoliubov transformation  $\hat{c}_k = u_k \hat{\gamma}_k + iv_k \hat{\gamma}_{-k}$ , and then splitting the sum  $\sum_k$  into the positive and negative parts  $\sum_{k>0} + \sum_{k<0}$ , we rewrite  $\hat{A}_i$  and  $\hat{B}_i$  as

$$\hat{A}_i = \hat{a}_i^\dagger + \hat{a}_i, \quad (\text{A36})$$

$$\hat{B}_i = \hat{b}_i^\dagger - \hat{b}_i \quad (\text{A37})$$

with

$$\hat{a}_i = \frac{1}{\sqrt{L}} \sum_{k>0} [e^{ikrj} (u_k - iv_k) \hat{\gamma}_k + e^{-ikrj} (u_k + iv_k) \hat{\gamma}_{-k}], \quad (\text{A38})$$

$$\hat{b}_i = \frac{1}{\sqrt{L}} \sum_{k>0} [e^{ikrj} (u_k + iv_k) \hat{\gamma}_k + e^{-ikrj} (u_k - iv_k) \hat{\gamma}_{-k}]. \quad (\text{A39})$$

The operators  $\hat{a}_i$  and  $\hat{b}_i$  satisfy

$$\langle \{\hat{a}_i, \hat{a}_j\} \rangle = \langle \{\hat{b}_i, \hat{b}_j\} \rangle = \langle \{\hat{a}_i, \hat{b}_j\} \rangle = 0, \quad (\text{A40})$$

$$\langle \{\hat{a}_i, \hat{a}_j^\dagger\} \rangle = \langle \{\hat{b}_i, \hat{b}_j^\dagger\} \rangle = \delta_{ij}, \quad (\text{A41})$$

$$\langle \{\hat{a}_i, \hat{b}_j^\dagger\} \rangle = \langle \{\hat{a}_i^\dagger, \hat{b}_j\} \rangle =: -G_{i-j}^{ab} \quad (\text{A42})$$

with

$$G_{i-j}^{ab} = -\frac{1}{\sqrt{L}} \sum_{k>0} [e^{ik(r_i - r_j)} (u_k - iv_k)^2 + e^{-ik(r_i - r_j)} (u_k + iv_k)^2]. \quad (\text{A43})$$

After the quench, the Heisenberg equation for  $\hat{c}_k(t)$  is given as

$$i \frac{d}{dt} \hat{c}_k(t) = -2\tilde{a}'_k \hat{c}_k(t) - 2i\tilde{b}'_k \hat{c}_{-k}^\dagger(t), \quad (\text{A44})$$

$$\tilde{a}'_k = g + \cos k, \quad (\text{A45})$$

$$\tilde{b}'_k = \sin k, \quad (\text{A46})$$

where the prime symbols indicate the parameters after the quench. As in the static case, we can introduce  $\tilde{u}_k(t)$  and  $\tilde{v}_k(t)$  for the Bogoliubov transformation at time  $t$

$$\begin{pmatrix} \hat{c}_k(t) \\ \hat{c}_{-k}^\dagger(t) \end{pmatrix} = \begin{pmatrix} \tilde{u}_k(t) & -\tilde{v}_k^*(t) \\ \tilde{v}_k(t) & \tilde{u}_k^*(t) \end{pmatrix} \begin{pmatrix} \hat{\gamma}_k \\ \hat{\gamma}_{-k}^\dagger \end{pmatrix} \quad (\text{A47})$$

satisfying

$$\tilde{u}_{-k}(t) = \tilde{u}_k(t), \quad (\text{A48})$$

$$\tilde{v}_{-k}(t) = -\tilde{v}_k(t), \quad (\text{A49})$$

$$|\tilde{u}_k(t)|^2 + |\tilde{v}_k(t)|^2 = 1. \quad (\text{A50})$$

Here  $\hat{\gamma}_k$  corresponds to the Bogoliubov excitations before the quench. From Eqs. (A44) and (A47),  $\tilde{u}_k(t)$  and  $\tilde{v}_k(t)$  should satisfy

$$i \frac{d}{dt} \begin{pmatrix} \tilde{u}_k(t) \\ \tilde{v}_k(t) \end{pmatrix} = \begin{pmatrix} -2\tilde{a}'_k & -2i\tilde{b}'_k \\ 2i\tilde{b}'_k & 2\tilde{a}'_k \end{pmatrix} \begin{pmatrix} \tilde{u}_k(t) \\ \tilde{v}_k(t) \end{pmatrix}. \quad (\text{A51})$$

Then, for the sudden quench ( $g_0 \rightarrow g$ ),  $\tilde{u}_k(t)$  and  $\tilde{v}_k(t)$  are explicitly given as

$$\begin{pmatrix} \tilde{u}_k(t) \\ \tilde{v}_k(t) \end{pmatrix} = \begin{pmatrix} u_k \cos 2\omega'_k t + i \frac{\tilde{a}'_k u_k + \tilde{b}'_k v_k}{\omega'_k} \sin 2\omega'_k t \\ -i v_k \cos 2\omega'_k t + \frac{\tilde{b}'_k u_k - \tilde{a}'_k v_k}{\omega'_k} \sin 2\omega'_k t \end{pmatrix}, \quad (\text{A52})$$

where each variable is represented as

$$\tilde{a}_k = g_0 + \cos k, \quad (\text{A53})$$

$$\tilde{b}_k = \sin k, \quad (\text{A54})$$

$$\omega_k = \sqrt{g_0^2 + 2g_0 \cos k + 1}, \quad (\text{A55})$$

$$\omega'_k = \sqrt{g^2 + 2g \cos k + 1}, \quad (\text{A56})$$

and Eqs. (A45) and (A46). The parameters  $u_k$  and  $v_k$  are defined in Eqs. (A15) and (A16).

As in the case of  $t = 0$ , the Heisenberg representation of each operator satisfies

$$\hat{A}_i(t) = \hat{a}_i^\dagger(t) + \hat{a}_i(t), \quad (\text{A57})$$

$$\hat{B}_i(t) = \hat{b}_i^\dagger(t) - \hat{b}_i(t) \quad (\text{A58})$$

with

$$\begin{aligned} \hat{a}_i(t) &= \frac{1}{\sqrt{L}} \sum_{k>0} \{ e^{ikr_j} [\tilde{u}_k(t) + \tilde{v}_k(t)] \hat{\gamma}_k \\ &\quad + e^{-ikr_j} [\tilde{u}_k(t) - \tilde{v}_k(t)] \hat{\gamma}_{-k} \}, \end{aligned} \quad (\text{A59})$$

$$\begin{aligned} \hat{b}_i(t) &= \frac{1}{\sqrt{L}} \sum_{k>0} \{ e^{ikr_j} [\tilde{u}_k(t) - \tilde{v}_k(t)] \hat{\gamma}_k \\ &\quad + e^{-ikr_j} [\tilde{u}_k(t) + \tilde{v}_k(t)] \hat{\gamma}_{-k} \}. \end{aligned} \quad (\text{A60})$$

Note that  $\hat{a}_i(t) \neq e^{i\hat{H}'t} \hat{a}_i e^{-i\hat{H}'t}$  and  $\hat{b}_i(t) \neq e^{i\hat{H}'t} \hat{b}_i e^{-i\hat{H}'t}$  in our notation. Then, the commutation relations for the operators are

$$\langle \{ \hat{a}_i(t), \hat{a}_j(t) \} \rangle = \langle \{ \hat{b}_i(t), \hat{b}_j(t) \} \rangle = \langle \{ \hat{a}_i(t), \hat{b}_j(t) \} \rangle = 0, \quad (\text{A61})$$

$$\langle \{ \hat{a}_i(t), \hat{a}_j^\dagger(t) \} \rangle = -G_{i-j}^{aa}(t), \quad (\text{A62})$$

$$\langle \{ \hat{b}_i(t), \hat{b}_j^\dagger(t) \} \rangle = -G_{i-j}^{bb}(t), \quad (\text{A63})$$

$$\langle \{ \hat{a}_i(t), \hat{b}_j^\dagger(t) \} \rangle = \langle \{ \hat{a}_i^\dagger(t), \hat{b}_j(t) \} \rangle = -G_{i-j}^{ab}(t) \quad (\text{A64})$$

with

$$\begin{aligned} G_{i-j}^{aa}(t) &= -\frac{2}{L} \sum_{k>0} \{ \cos[k(r_i - r_j)] [|\tilde{u}_k(t)|^2 + |\tilde{v}_k(t)|^2] \\ &\quad + i \sin[k(r_i - r_j)] [\tilde{u}_k(t) \tilde{v}_k^*(t) + \tilde{v}_k(t) \tilde{u}_k^*(t)] \}, \end{aligned} \quad (\text{A65})$$

$$\begin{aligned} G_{i-j}^{bb}(t) &= -\frac{2}{L} \sum_{k>0} \{ \cos[k(r_i - r_j)] [|\tilde{u}_k(t)|^2 + |\tilde{v}_k(t)|^2] \\ &\quad - i \sin[k(r_i - r_j)] [\tilde{u}_k(t) \tilde{v}_k^*(t) + \tilde{v}_k(t) \tilde{u}_k^*(t)] \}, \end{aligned} \quad (\text{A66})$$

$$G_{i-j}^{ab}(t) = -\frac{2}{L} \sum_{k>0} \{ \cos[k(r_i - r_j)] [|\tilde{u}_k(t)|^2 - |\tilde{v}_k(t)|^2] \}$$

$$-i \sin[k(r_i - r_j)] [\tilde{u}_k(t) \tilde{v}_k^*(t) - \tilde{v}_k(t) \tilde{u}_k^*(t)] \}. \quad (\text{A67})$$

Using these results, we obtain

$$S_{0,r} = \langle \hat{B}_0(t) \hat{B}_r(t) \rangle = -\langle \{ \hat{b}_0(t), \hat{b}_r^\dagger(t) \} \rangle = +G_{-r}^{bb}(t), \quad (\text{A68})$$

$$Q_{0,r} = \langle \hat{A}_0(t) \hat{A}_r(t) \rangle = +\langle \{ \hat{a}_0(t), \hat{a}_r^\dagger(t) \} \rangle = -G_{-r}^{aa}(t), \quad (\text{A69})$$

$$G_{0,r} = \langle \hat{B}_0(t) \hat{A}_r(t) \rangle = -\langle \{ \hat{b}_0(t), \hat{a}_r^\dagger(t) \} \rangle = +G_{+r}^{ab}(t). \quad (\text{A70})$$

## 5. Maximum group velocity

In the 1D transverse-field Ising model, the Lieb-Robinson velocity is obtained as the maximum group velocity determined from the derivative of the band dispersion [50–53]. It is given as

$$v^{\text{LR}} = \max_k \left| \frac{d\omega_k}{dk} \right| = \begin{cases} 2\tilde{g} & \text{if } \tilde{g} \leq 1 \\ 2 & \text{if } \tilde{g} \geq 1 \end{cases} \quad (\text{A71})$$

for the Hamiltonian defined in Eq. (A1), and it is obtained as

$$v^{\text{LR}} = \begin{cases} \Gamma & \text{if } \Gamma \leq J/2 \\ J/2 & \text{if } \Gamma \geq J/2 \end{cases} \quad (\text{A72})$$

for the original Hamiltonian given in Eq. (1).

## Appendix B: Details of the LSWA

### 1. Bosonic quadratic Hamiltonian

We consider a sudden quench within the disordered phase for the Hamiltonian in Eq. (1). We investigate the effect of small quantum fluctuations around the completely disordered state at  $\Gamma \rightarrow \infty$  using a linear spin-wave expansion [64–68]. As long as we consider a quench to a strong transverse field so that the transverse magnetization is large enough ( $\langle S_i^x \rangle \approx 1/2$ ), this approach should be a good approximation. We specifically study the parameter region  $\Gamma \in (\Gamma_c^{\text{classical}}, \infty)$ , where the classical transition point obtained by the mean-field approximation [17, 114, 115] is  $\Gamma_c^{\text{classical}} = JD$  with  $D$  being the spatial dimension. We review the derivation of the longitudinal correlation functions [65] and then calculate the transverse correlation functions, which have not been investigated in previous studies.

We apply the linearized Holstein-Primakoff transformation, which is given as

$$\hat{S}_i^x = S - \hat{b}_i^\dagger \hat{b}_i, \quad \hat{S}_i^z = \frac{\sqrt{2S}}{2} (\hat{b}_i^\dagger + \hat{b}_i) \quad (\text{B1})$$

before the quench and is represented as

$$\hat{S}_i^{x'} = S - \hat{a}_i^\dagger \hat{a}_i, \quad \hat{S}_i^{z'} = \frac{\sqrt{2S}}{2} (\hat{a}_i^\dagger + \hat{a}_i) \quad (\text{B2})$$

after the quench. The prime symbols indicate operators after the quench. After the Fourier transformation ( $\hat{b}_i = \frac{1}{\sqrt{LD}} \sum_{\mathbf{k}} e^{-i\mathbf{k}\cdot\mathbf{r}_i} \hat{b}_{\mathbf{k}}$ ,  $\hat{a}_i = \frac{1}{\sqrt{LD}} \sum_{\mathbf{k}} e^{-i\mathbf{k}\cdot\mathbf{r}_i} \hat{a}_{\mathbf{k}}$ ) and the Bogoliubov transformation, we obtain the Hamiltonian for free bosons before the quench (up to constant terms) as

$$\hat{H} = \sum_{\mathbf{k}} \Omega_{\mathbf{k}} \hat{\beta}_{\mathbf{k}}^\dagger \hat{\beta}_{\mathbf{k}}, \quad (\text{B3})$$

$$\hat{b}_{\mathbf{k}} = s_{\mathbf{k}} \hat{\beta}_{\mathbf{k}} + t_{\mathbf{k}} \hat{\beta}_{-\mathbf{k}}^\dagger, \quad (\text{B4})$$

and that after the quench (up to constant terms) as

$$\hat{H}' = \sum_{\mathbf{k}} \Omega'_{\mathbf{k}} \hat{\alpha}_{\mathbf{k}}^\dagger \hat{\alpha}_{\mathbf{k}}, \quad (\text{B5})$$

$$\hat{a}_{\mathbf{k}} = s'_{\mathbf{k}} \hat{\alpha}_{\mathbf{k}} + t'_{\mathbf{k}} \hat{\alpha}_{-\mathbf{k}}^\dagger. \quad (\text{B6})$$

Here the corresponding dispersions and coefficients are defined as

$$\Omega_{\mathbf{k}} = \text{sgn}(A_{\mathbf{k}}) \sqrt{A_{\mathbf{k}}^2 - B_{\mathbf{k}}^2}, \quad (\text{B7})$$

$$s_{\mathbf{k}} = \text{sgn}(A_{\mathbf{k}}) \sqrt{\frac{1}{2} \left( \frac{|A_{\mathbf{k}}|}{|\Omega_{\mathbf{k}}|} + 1 \right)}, \quad (\text{B8})$$

$$t_{\mathbf{k}} = -\text{sgn}(B_{\mathbf{k}}) \sqrt{\frac{1}{2} \left( \frac{|A_{\mathbf{k}}|}{|\Omega_{\mathbf{k}}|} - 1 \right)}, \quad (\text{B9})$$

$$\Omega'_{\mathbf{k}} = \text{sgn}(A'_{\mathbf{k}}) \sqrt{A'_{\mathbf{k}}{}^2 - B'_{\mathbf{k}}{}^2}, \quad (\text{B10})$$

$$s'_{\mathbf{k}} = \text{sgn}(A'_{\mathbf{k}}) \sqrt{\frac{1}{2} \left( \frac{|A'_{\mathbf{k}}|}{|\Omega'_{\mathbf{k}}|} + 1 \right)}, \quad (\text{B11})$$

$$t'_{\mathbf{k}} = -\text{sgn}(B'_{\mathbf{k}}) \sqrt{\frac{1}{2} \left( \frac{|A'_{\mathbf{k}}|}{|\Omega'_{\mathbf{k}}|} - 1 \right)}, \quad (\text{B12})$$

where

$$A_{\mathbf{k}} = -\frac{z}{2} JS\gamma_{\mathbf{k}} + \Gamma, \quad B_{\mathbf{k}} = -\frac{z}{2} JS\gamma_{\mathbf{k}}, \quad (\text{B13})$$

$$A'_{\mathbf{k}} = -\frac{z}{2} J'S\gamma_{\mathbf{k}} + \Gamma', \quad B'_{\mathbf{k}} = -\frac{z}{2} J'S\gamma_{\mathbf{k}}, \quad (\text{B14})$$

$$\gamma_{\mathbf{k}} = \frac{1}{D} \sum_{\nu=1}^D \cos k_{\nu} \quad (\text{B15})$$

with  $z = 2D$  being the coordination number. We add the prime symbols to distinguish parameters after the quench.

At  $t = 0$ , the vacuum of both Hamiltonians are the same, and bosons before the Holstein-Primakoff transformation satisfy  $\hat{b}_{\mathbf{k}} = \hat{a}_{\mathbf{k}}$ . Then, these operators should fulfill

$$\begin{aligned} \begin{pmatrix} \hat{b}_{\mathbf{k}} \\ \hat{b}_{-\mathbf{k}}^\dagger \end{pmatrix} &= \begin{pmatrix} s_{\mathbf{k}} & t_{\mathbf{k}} \\ t_{\mathbf{k}} & s_{\mathbf{k}} \end{pmatrix} \begin{pmatrix} \hat{\beta}_{\mathbf{k}} \\ \hat{\beta}_{-\mathbf{k}}^\dagger \end{pmatrix} \\ &= \begin{pmatrix} s'_{\mathbf{k}} & t'_{\mathbf{k}} \\ t'_{\mathbf{k}} & s'_{\mathbf{k}} \end{pmatrix} \begin{pmatrix} \hat{\alpha}_{\mathbf{k}} \\ \hat{\alpha}_{-\mathbf{k}}^\dagger \end{pmatrix} = \begin{pmatrix} \hat{a}_{\mathbf{k}} \\ \hat{a}_{-\mathbf{k}}^\dagger \end{pmatrix}. \end{aligned} \quad (\text{B16})$$

This means that Bogoliubov excitations before and after the quench are connected by

$$\begin{aligned} \begin{pmatrix} \hat{\alpha}_{\mathbf{k}} \\ \hat{\alpha}_{-\mathbf{k}}^\dagger \end{pmatrix} &= \begin{pmatrix} s'_{\mathbf{k}} s_{\mathbf{k}} - t'_{\mathbf{k}} t_{\mathbf{k}} & s'_{\mathbf{k}} t_{\mathbf{k}} - s_{\mathbf{k}} t'_{\mathbf{k}} \\ s'_{\mathbf{k}} t_{\mathbf{k}} - s_{\mathbf{k}} t'_{\mathbf{k}} & s'_{\mathbf{k}} s_{\mathbf{k}} - t'_{\mathbf{k}} t_{\mathbf{k}} \end{pmatrix} \begin{pmatrix} \hat{\beta}_{\mathbf{k}} \\ \hat{\beta}_{-\mathbf{k}}^\dagger \end{pmatrix} \\ &=: \begin{pmatrix} u_{\mathbf{k}} & v_{\mathbf{k}} \\ v_{\mathbf{k}} & u_{\mathbf{k}} \end{pmatrix} \begin{pmatrix} \hat{\beta}_{\mathbf{k}} \\ \hat{\beta}_{-\mathbf{k}}^\dagger \end{pmatrix}, \end{aligned} \quad (\text{B17})$$

where the coefficients satisfy

$$u_{\mathbf{k}}^2 - v_{\mathbf{k}}^2 = s'_{\mathbf{k}}{}^2 - t'_{\mathbf{k}}{}^2 = s_{\mathbf{k}}^2 - t_{\mathbf{k}}^2 = 1. \quad (\text{B18})$$

## 2. Longitudinal correlation functions

We evaluate the time-dependent longitudinal correlation functions defined as

$$C^{zz}(\mathbf{r}, t) = \langle \psi_0 | e^{i\hat{H}'t} \hat{S}_{\mathbf{r}}^z \hat{S}_{\mathbf{0}}^z e^{-i\hat{H}'t} | \psi_0 \rangle \quad (\text{B19})$$

$$= \frac{S}{2} \langle \psi_0 | e^{i\hat{H}'t} (\hat{b}_{\mathbf{r}}^\dagger + \hat{b}_{\mathbf{r}}) (\hat{b}_{\mathbf{0}}^\dagger + \hat{b}_{\mathbf{0}}) e^{-i\hat{H}'t} | \psi_0 \rangle. \quad (\text{B20})$$

Writing them in the Fourier space ( $\hat{b}_i = \frac{1}{\sqrt{LD}} \sum_{\mathbf{k}} e^{-i\mathbf{k}\cdot\mathbf{r}_i} \hat{b}_{\mathbf{k}}$ ) and in the Heisenberg picture, we obtain

$$\begin{aligned} C^{zz}(\mathbf{r}, t) &= \frac{S}{2LD} \sum_{\mathbf{k}} e^{i\mathbf{k}\cdot\mathbf{r}} \langle \psi_0 | [\hat{b}_{\mathbf{k}}^\dagger(t) \hat{b}_{-\mathbf{k}}^\dagger(t) + \hat{b}_{\mathbf{k}}^\dagger(t) \hat{b}_{\mathbf{k}}(t) \\ &\quad + \hat{b}_{-\mathbf{k}}(t) \hat{b}_{-\mathbf{k}}^\dagger(t) + \hat{b}_{-\mathbf{k}}(t) \hat{b}_{\mathbf{k}}(t)] | \psi_0 \rangle. \end{aligned} \quad (\text{B21})$$

We then replace all operators  $\hat{b}_{\mathbf{k}}(t)$  by  $\hat{\beta}_{\mathbf{k}}$ . Because  $\hat{b}_{\mathbf{k}}(t) = s'_{\mathbf{k}} \hat{\alpha}_{\mathbf{k}}(t) + t'_{\mathbf{k}} \hat{\alpha}_{-\mathbf{k}}^\dagger(t)$ ,  $\hat{\alpha}_{\mathbf{k}}(t) = e^{-i\Omega'_{\mathbf{k}}t} \hat{\alpha}_{\mathbf{k}}$ , and  $\hat{\alpha}_{\mathbf{k}} = u_{\mathbf{k}} \hat{\beta}_{\mathbf{k}} + v_{\mathbf{k}} \hat{\beta}_{-\mathbf{k}}^\dagger$ , the following relation holds:

$$\begin{aligned} \hat{b}_{\mathbf{k}}(t) &= (e^{-i\Omega'_{\mathbf{k}}t} s'_{\mathbf{k}} u_{\mathbf{k}} + e^{+i\Omega'_{\mathbf{k}}t} t'_{\mathbf{k}} v_{\mathbf{k}}) \hat{\beta}_{\mathbf{k}} \\ &\quad + (e^{-i\Omega'_{\mathbf{k}}t} s'_{\mathbf{k}} v_{\mathbf{k}} + e^{+i\Omega'_{\mathbf{k}}t} t'_{\mathbf{k}} u_{\mathbf{k}}) \hat{\beta}_{-\mathbf{k}}^\dagger. \end{aligned} \quad (\text{B22})$$

After straightforward calculations using  $\hat{\beta}_{\mathbf{k}}|\psi_0\rangle = 0$ , we obtain

$$\begin{aligned} C^{zz}(\mathbf{r}, t) &= \frac{S}{2LD} \sum_{\mathbf{k}} e^{i\mathbf{k}\cdot\mathbf{r}} (s'_{\mathbf{k}} + t'_{\mathbf{k}})^2 \\ &\quad \cdot (u_{\mathbf{k}}^2 + v_{\mathbf{k}}^2 + 2u_{\mathbf{k}}v_{\mathbf{k}} \cos 2\Omega'_{\mathbf{k}}t). \end{aligned} \quad (\text{B23})$$

Substituting  $u_{\mathbf{k}}$  and  $v_{\mathbf{k}}$  with  $s_{\mathbf{k}}$ ,  $s'_{\mathbf{k}}$ ,  $t_{\mathbf{k}}$ , and  $t'_{\mathbf{k}}$  using Eq. (B17), we get

$$C^{zz}(\mathbf{r}, 0) = \frac{S}{2LD} \sum_{\mathbf{k}} e^{i\mathbf{k}\cdot\mathbf{r}} (s'_{\mathbf{k}} + t'_{\mathbf{k}})^2 (u_{\mathbf{k}} + v_{\mathbf{k}})^2 \quad (\text{B24})$$

$$= \frac{S}{2LD} \sum_{\mathbf{k}} e^{i\mathbf{k}\cdot\mathbf{r}} (s_{\mathbf{k}} + t_{\mathbf{k}})^2, \quad (\text{B25})$$

$$\tilde{C}^{zz}(\mathbf{r}, t) := C^{zz}(\mathbf{r}, t) - C^{zz}(\mathbf{r}, 0) \quad (\text{B26})$$

$$= \frac{S}{2L^D} \sum_{\mathbf{k}} e^{i\mathbf{k}\cdot\mathbf{r}} (s'_k + t'_k)^2 2u_k v_k (\cos 2\Omega'_k t - 1) \quad (\text{B27})$$

$$= \frac{S}{2L^D} \sum_{\mathbf{k}} e^{i\mathbf{k}\cdot\mathbf{r}} (-2)[(s_k^2 + t_k^2)s'_k t'_k - (s_k'^2 + t_k'^2)s_k t_k](s'_k + t'_k)^2 (\cos 2\Omega'_k t - 1). \quad (\text{B28})$$

Using the relations defined in Eqs. (B7-B15), we finally get [65]

$$C^{zz}(\mathbf{r}, 0) = \frac{S}{2L^D} \sum_{\mathbf{k}} e^{i\mathbf{k}\cdot\mathbf{r}} \frac{\Omega_{\mathbf{k}}}{A_{\mathbf{k}} + B_{\mathbf{k}}}, \quad (\text{B29})$$

$$\tilde{C}^{zz}(\mathbf{r}, t) = \frac{S}{2L^D} \sum_{\mathbf{k}} e^{i\mathbf{k}\cdot\mathbf{r}} \frac{A_{\mathbf{k}} B'_{\mathbf{k}} - A'_{\mathbf{k}} B_{\mathbf{k}}}{\Omega_{\mathbf{k}}(A'_{\mathbf{k}} + B'_{\mathbf{k}})} (\cos 2\Omega'_k t - 1). \quad (\text{B30})$$

For  $\Gamma \rightarrow \infty$  before the quench,  $\Omega_{\mathbf{k}}/(A_{\mathbf{k}} + B_{\mathbf{k}}) = 1$  is satisfied, and hence,  $C^{zz}(\mathbf{r}, 0) = S/2 \times \delta_{\mathbf{r}, L\mathbf{m}}$  ( $m_{\nu}$ : integer,  $\nu = 1, 2, \dots, D$ ) holds. This means that  $C^{zz}(\mathbf{r}, t) = \tilde{C}^{zz}(\mathbf{r}, t)$  for  $1 \leq r_{\nu} \leq L/2$  ( $\nu = 1, 2, \dots, D$ ). Besides, when  $J = 0$  and  $J' \ll \Gamma' < \Gamma$ , the intensity of the correlation would be approximately  $|C^{zz}(\mathbf{r}, t)| = \mathcal{O}[S/L^D \times \sum_{\mathbf{k}} B'_{\mathbf{k}}/(A'_{\mathbf{k}} + B'_{\mathbf{k}})] = \mathcal{O}(zS^2 J'/\Gamma')$ .

### 3. Transverse correlation functions

We evaluate the time-dependent transverse correlation functions defined as

$$C^{xx}(\mathbf{r}, t) = \langle \psi_0 | e^{i\hat{H}'t} \hat{S}_{\mathbf{r}} \hat{S}_{\mathbf{0}} e^{-i\hat{H}'t} | \psi_0 \rangle \quad (\text{B31})$$

$$= \langle \psi_0 | e^{i\hat{H}'t} (S - \hat{b}_{\mathbf{r}} \hat{b}_{\mathbf{r}}) (S - \hat{b}_{\mathbf{0}} \hat{b}_{\mathbf{0}}) e^{-i\hat{H}'t} | \psi_0 \rangle \quad (\text{B32})$$

and the connected one defined as

$$C_{\text{connected}}^{xx}(\mathbf{r}, t) = C^{xx}(\mathbf{r}, t) - \langle \psi_0 | e^{i\hat{H}'t} \hat{S}_{\mathbf{r}} e^{-i\hat{H}'t} | \psi_0 \rangle \cdot \langle \psi_0 | e^{i\hat{H}'t} \hat{S}_{\mathbf{0}} e^{-i\hat{H}'t} | \psi_0 \rangle. \quad (\text{B33})$$

Writing them in the Fourier space ( $\hat{b}_i = \frac{1}{\sqrt{L^D}} \sum_{\mathbf{k}} e^{-i\mathbf{k}\cdot\mathbf{r}_i} \hat{b}_{\mathbf{k}}$ ) and in the Heisenberg picture, we obtain

$$C^{xx}(\mathbf{r}, t) = S^2 - \frac{2S}{L^D} \sum_{\mathbf{k}} \langle \psi_0 | \hat{b}_{\mathbf{k}}^{\dagger}(t) \hat{b}_{\mathbf{k}}(t) | \psi_0 \rangle + \frac{1}{L^{2D}} \sum_{\mathbf{k}, \mathbf{l}, \mathbf{p}} e^{i(\mathbf{k}-\mathbf{l})\cdot\mathbf{r}} \langle \psi_0 | \hat{b}_{\mathbf{k}}^{\dagger}(t) \hat{b}_{\mathbf{l}}(t) \hat{b}_{\mathbf{p}}^{\dagger}(t) \hat{b}_{\mathbf{k}-\mathbf{l}+\mathbf{p}}(t) | \psi_0 \rangle \quad (\text{B34})$$

and

$$C_{\text{connected}}^{xx}(\mathbf{r}, t) = - \left[ \frac{1}{L^D} \sum_{\mathbf{k}} \langle \psi_0 | \hat{b}_{\mathbf{k}}^{\dagger}(t) \hat{b}_{\mathbf{k}}(t) | \psi_0 \rangle \right]^2 + \frac{1}{L^{2D}} \sum_{\mathbf{k}, \mathbf{l}, \mathbf{p}} e^{i(\mathbf{k}-\mathbf{l})\cdot\mathbf{r}} \langle \psi_0 | \hat{b}_{\mathbf{k}}^{\dagger}(t) \hat{b}_{\mathbf{l}}(t) \hat{b}_{\mathbf{p}}^{\dagger}(t) \hat{b}_{\mathbf{k}-\mathbf{l}+\mathbf{p}}(t) | \psi_0 \rangle. \quad (\text{B35})$$

As in the case of longitudinal correlation functions, we replace  $\hat{b}_{\mathbf{k}}(t)$  by  $\hat{\beta}_{\mathbf{k}}$  and use  $\hat{\beta}_{\mathbf{k}}|\psi_0\rangle = 0$ . Non-vanishing terms contain  $\langle \psi_0 | \hat{\beta}_{-\mathbf{k}} \hat{\beta}_{-\mathbf{l}} \hat{\beta}_{-\mathbf{p}} \hat{\beta}_{-(\mathbf{k}-\mathbf{l}+\mathbf{p})} | \psi_0 \rangle = \delta_{\mathbf{k}, \mathbf{l}}$ ,  $\langle \psi_0 | \hat{\beta}_{-\mathbf{k}} \hat{\beta}_{\mathbf{l}} \hat{\beta}_{\mathbf{p}} \hat{\beta}_{-(\mathbf{k}-\mathbf{l}+\mathbf{p})} | \psi_0 \rangle = \delta_{\mathbf{k}, -\mathbf{p}} + \delta_{\mathbf{l}, \mathbf{p}}$ , and  $\langle \psi_0 | \hat{\beta}_{-\mathbf{k}} \hat{\beta}_{-\mathbf{k}} | \psi_0 \rangle = 1$ . After straightforward calculations, we get

$$\frac{1}{L^D} \sum_{\mathbf{k}} \langle \psi_0 | \hat{b}_{\mathbf{k}}^{\dagger}(t) \hat{b}_{\mathbf{k}}(t) | \psi_0 \rangle = \frac{1}{L^D} \sum_{\mathbf{k}} (s_k'^2 v_k^2 + t_k'^2 u_k^2 + 2s_k' t_k' u_k v_k \cos 2\Omega'_k t) \quad (\text{B36})$$

$$= \frac{1}{L^D} \sum_{\mathbf{k}} [t_k^2 + 2s_k' t_k' u_k v_k (\cos 2\Omega'_k t - 1)] \quad (\text{B37})$$

and

$$C_{\text{connected}}^{xx}(\mathbf{r}, t) = \left| \frac{1}{L^D} \sum_{\mathbf{k}} e^{i\mathbf{k}\cdot\mathbf{r}} \left\{ [(s_k'^2 + t_k'^2) \cos 2\Omega'_k t + i \sin 2\Omega'_k t] u_k v_k + s_k' t_k' (u_k^2 + v_k^2) \right\} \right|^2 + \frac{1}{L^{2D}} \sum_{\mathbf{k}, \mathbf{l}} e^{i(\mathbf{k}-\mathbf{l})\cdot\mathbf{r}} [t_k^2 + 2s_k' t_k' u_k v_k (\cos 2\Omega'_k t - 1)] [s_l^2 + 2s_l' t_l' u_l v_l (\cos 2\Omega'_l t - 1)] \quad (\text{B38})$$

$$= \left| \frac{1}{L^D} \sum_{\mathbf{k}} e^{i\mathbf{k}\cdot\mathbf{r}} \left\{ [(s_k'^2 + t_k'^2) \cos 2\Omega'_k t + i \sin 2\Omega'_k t] u_k v_k + s_k' t_k' (u_k^2 + v_k^2) \right\} \right|^2 + \left| \frac{1}{L^D} \sum_{\mathbf{k}} e^{i\mathbf{k}\cdot\mathbf{r}} [t_k^2 + 2s_k' t_k' u_k v_k (\cos 2\Omega'_k t - 1)] \right|^2$$

$$+ \frac{1}{L^D} \sum_{\mathbf{k}} [t_{\mathbf{k}}^2 + 2s'_{\mathbf{k}} t'_{\mathbf{k}} u_{\mathbf{k}} v_{\mathbf{k}} (\cos 2\Omega'_{\mathbf{k}} t - 1)] \times \delta_{\mathbf{r}, Lm} \quad (\text{B39})$$

with  $m_{\nu}$  ( $\nu = 1, 2, \dots, D$ ) being integer. Substituting the parameters  $u_{\mathbf{k}}, v_{\mathbf{k}}, s_{\mathbf{k}}, t_{\mathbf{k}}, s'_{\mathbf{k}},$  and  $t'_{\mathbf{k}}$  with the parameters  $A_{\mathbf{k}}, B_{\mathbf{k}}, \Omega_{\mathbf{k}}, A'_{\mathbf{k}}, B'_{\mathbf{k}},$  and  $\Omega'_{\mathbf{k}},$  we finally get

$$\left[ -\frac{B'_{\mathbf{k}} A_{\mathbf{k}} B'_{\mathbf{k}} - A'_{\mathbf{k}} B_{\mathbf{k}}}{2 \Omega_{\mathbf{k}} \Omega'^2_{\mathbf{k}}} \cos 2\Omega'_{\mathbf{k}} t \right] \quad (\text{B40})$$

$$\begin{aligned} & \frac{1}{L^D} \sum_{\mathbf{k}} \langle \psi_0 | \hat{b}_{\mathbf{k}}^{\dagger}(t) \hat{b}_{\mathbf{k}}(t) | \psi_0 \rangle \\ &= \frac{1}{L^D} \sum_{\mathbf{k}} e^{i\mathbf{k} \cdot \mathbf{r}} \left[ \left( \frac{A'_{\mathbf{k}} A_{\mathbf{k}} A'_{\mathbf{k}} - B_{\mathbf{k}} B'_{\mathbf{k}}}{2 \Omega_{\mathbf{k}} \Omega'^2_{\mathbf{k}}} - \frac{1}{2} \right) \right. \\ & \quad \left. - \frac{B'_{\mathbf{k}} A_{\mathbf{k}} B'_{\mathbf{k}} - A'_{\mathbf{k}} B_{\mathbf{k}}}{2 \Omega_{\mathbf{k}} \Omega'^2_{\mathbf{k}}} (\cos 2\Omega'_{\mathbf{k}} t - 1) \right] \quad (\text{B41}) \end{aligned}$$

and

$$\begin{aligned} C_{\text{connected}}^{xx}(\mathbf{r}, t) &= \left| \frac{1}{L^D} \sum_{\mathbf{k}} e^{i\mathbf{k} \cdot \mathbf{r}} \left[ -\frac{B'_{\mathbf{k}} A_{\mathbf{k}} A'_{\mathbf{k}} - B_{\mathbf{k}} B'_{\mathbf{k}}}{2 \Omega_{\mathbf{k}} \Omega'^2_{\mathbf{k}}} + \frac{A_{\mathbf{k}} B'_{\mathbf{k}} - A'_{\mathbf{k}} B_{\mathbf{k}}}{2 \Omega_{\mathbf{k}} \Omega'_{\mathbf{k}}} \left( \frac{A'_{\mathbf{k}}}{\Omega'_{\mathbf{k}}} \cos 2\Omega'_{\mathbf{k}} t + i \sin 2\Omega'_{\mathbf{k}} t \right) \right] \right|^2 \\ &+ \left| \frac{1}{L^D} \sum_{\mathbf{k}} e^{i\mathbf{k} \cdot \mathbf{r}} \left[ \left( \frac{A'_{\mathbf{k}} A_{\mathbf{k}} A'_{\mathbf{k}} - B_{\mathbf{k}} B'_{\mathbf{k}}}{2 \Omega_{\mathbf{k}} \Omega'^2_{\mathbf{k}}} - \frac{1}{2} \right) - \frac{B'_{\mathbf{k}} A_{\mathbf{k}} B'_{\mathbf{k}} - A'_{\mathbf{k}} B_{\mathbf{k}}}{2 \Omega_{\mathbf{k}} \Omega'^2_{\mathbf{k}}} \cos 2\Omega'_{\mathbf{k}} t \right] \right|^2 \\ &+ \frac{1}{L^D} \sum_{\mathbf{k}} \left[ \left( \frac{A'_{\mathbf{k}} A_{\mathbf{k}} A'_{\mathbf{k}} - B_{\mathbf{k}} B'_{\mathbf{k}}}{2 \Omega_{\mathbf{k}} \Omega'^2_{\mathbf{k}}} - \frac{1}{2} \right) - \frac{B'_{\mathbf{k}} A_{\mathbf{k}} B'_{\mathbf{k}} - A'_{\mathbf{k}} B_{\mathbf{k}}}{2 \Omega_{\mathbf{k}} \Omega'^2_{\mathbf{k}}} \cos 2\Omega'_{\mathbf{k}} t \right] \times \delta_{\mathbf{r}, Lm} \quad (\text{B42}) \end{aligned}$$

$$\begin{aligned} &= \left| \frac{1}{L^D} \sum_{\mathbf{k}} e^{i\mathbf{k} \cdot \mathbf{r}} \left\{ -\frac{B_{\mathbf{k}}}{2\Omega_{\mathbf{k}}} + \frac{A_{\mathbf{k}} B'_{\mathbf{k}} - A'_{\mathbf{k}} B_{\mathbf{k}}}{2\Omega_{\mathbf{k}} \Omega'_{\mathbf{k}}} \left[ \frac{A'_{\mathbf{k}}}{\Omega'_{\mathbf{k}}} (\cos 2\Omega'_{\mathbf{k}} t - 1) + i \sin 2\Omega'_{\mathbf{k}} t \right] \right\} \right|^2 \\ &+ \left| \frac{1}{L^D} \sum_{\mathbf{k}} e^{i\mathbf{k} \cdot \mathbf{r}} \left[ \frac{1}{2} \left( \frac{A_{\mathbf{k}}}{\Omega_{\mathbf{k}}} - 1 \right) - \frac{B'_{\mathbf{k}} A_{\mathbf{k}} B'_{\mathbf{k}} - A'_{\mathbf{k}} B_{\mathbf{k}}}{2 \Omega_{\mathbf{k}} \Omega'^2_{\mathbf{k}}} (\cos 2\Omega'_{\mathbf{k}} t - 1) \right] \right|^2 \\ &+ \frac{1}{L^D} \sum_{\mathbf{k}} \left[ \frac{1}{2} \left( \frac{A_{\mathbf{k}}}{\Omega_{\mathbf{k}}} - 1 \right) - \frac{B'_{\mathbf{k}} A_{\mathbf{k}} B'_{\mathbf{k}} - A'_{\mathbf{k}} B_{\mathbf{k}}}{2 \Omega_{\mathbf{k}} \Omega'^2_{\mathbf{k}}} (\cos 2\Omega'_{\mathbf{k}} t - 1) \right] \times \delta_{\mathbf{r}, Lm} \quad (\text{B43}) \end{aligned}$$

with  $m_{\nu}$  ( $\nu = 1, 2, \dots, D$ ) being integer.

When  $J = 0$  and  $J' \ll \Gamma' < \Gamma$ , the intensity of the correlation would be approximately  $|C_{\text{connected}}^{xx}(\mathbf{r}, t)| = \mathcal{O}[1/L^D \times \sum_{\mathbf{k}} B'_{\mathbf{k}} A'_{\mathbf{k}} / (\Omega'_{\mathbf{k}})^2] = \mathcal{O}(z^2 S^2 J'^2 / \Gamma'^2)$ .

#### 4. Dispersion relation and maximum group velocity

Within the LSWA, the dispersion relation for  $S = 1/2$  is expressed as

$$\Omega_{\mathbf{k}} = \sqrt{\Gamma^2 - \frac{z}{2} \Gamma J \gamma_{\mathbf{k}}}, \quad (\text{B44})$$

$$= \Gamma \left\{ 1 - \frac{1}{2} \frac{zJ}{2\Gamma} \gamma_{\mathbf{k}} - \frac{1}{8} \left( \frac{zJ}{2\Gamma} \right)^2 \gamma_{\mathbf{k}}^2 + \mathcal{O} \left[ \left( \frac{zJ}{2\Gamma} \right)^3 \right] \right\}. \quad (\text{B45})$$

This result is consistent with the dispersion relation

$$\begin{aligned} \Omega_{\mathbf{k}}^{\text{perturb}} &= \Gamma \left\{ 1 - \frac{1}{2} \frac{zJ}{2\Gamma} \gamma_{\mathbf{k}} - \frac{1}{8} \left( \frac{zJ}{2\Gamma} \right)^2 \left( \gamma_{\mathbf{k}}^2 - \frac{2}{9} \right) \right. \\ &\quad \left. - \frac{1}{16} \left( \frac{zJ}{2\Gamma} \right)^3 \left( \gamma_{\mathbf{k}}^3 + \gamma_{\mathbf{k}} \frac{2-3z}{z^2} \right) + \mathcal{O} \left[ \left( \frac{zJ}{2\Gamma} \right)^4 \right] \right\} \quad (\text{B46}) \end{aligned}$$

obtained by the perturbation calculation [113] up to  $\mathcal{O}\{[(zJ)/(2\Gamma)]^2\}$  terms.

It is widely believed that the Lieb-Robinson velocity should be the maximum group velocity determined from the derivative of band dispersion [50–53]. Although the dispersion obtained by the LSWA does not necessarily offer the exact Lieb-Robinson velocity, we calculate the reference value using the dispersion. In 1D, the maximum

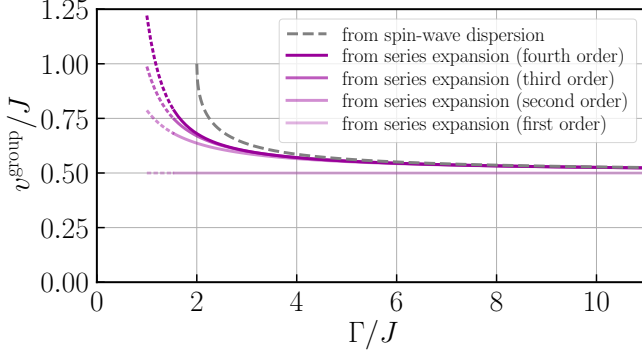


FIG. 23. Field dependence of the group velocity along the horizontal axis estimated from the dispersion relation obtained by the LSWA and the series expansion up to fourth order [116–118] in 2D. The group velocity is represented by the solid (dotted) lines above (below) the critical transverse field  $\Gamma_c/J \approx 1.522$  [17, 47, 48]. Both velocities increase with decreasing the transverse field.

group velocity of the spin-wave dispersion is given as

$$v^{\text{SW}} = \max_{\mathbf{k}} \left| \frac{d\Omega_{\mathbf{k}}}{dk} \right| = \frac{J}{\sqrt{2}} \left[ 1 + \sqrt{1 - \left( \frac{J}{\Gamma} \right)^2} \right]^{-1/2}. \quad (\text{B47})$$

For  $\Gamma \rightarrow \infty$ , the group velocity satisfies  $v^{\text{SW}} \rightarrow J/2 = v^{\text{LR}}$ , reproducing the exact maximum group velocity. On the other hand, for  $\Gamma \in (\Gamma_c^{\text{classical}}, \infty)$ , the LSWA always gives  $v^{\text{SW}} > J/2 = v^{\text{LR}}$ . Its worst (largest) estimate  $v^{\text{SW}} = J/\sqrt{2} \approx 0.707J$  at  $\Gamma = \Gamma_c^{\text{classical,1D}} (= J)$  is still tighter than the recent bound  $1.51J$  obtained by the general formula for the Lieb-Robinson bound [23].

In the same manner, we can extract the group velocity as  $v^{\text{SW}} = \max_{\mathbf{k}} \nabla_{\mathbf{k}} \Omega_{\mathbf{k}}$  from the spin-wave dispersion in higher dimensions. In 2D, the horizontal and diagonal velocities are given as

$$v^{\text{SW,horizontal}} = \frac{J}{\sqrt{2}} \left( 1 - \frac{J}{\Gamma} + \sqrt{1 - \frac{2J}{\Gamma}} \right)^{-1/2}, \quad (\text{B48})$$

$$v^{\text{SW,diagonal}} = J \left[ 1 + \sqrt{1 - \left( \frac{2J}{\Gamma} \right)^2} \right]^{-1/2}, \quad (\text{B49})$$

respectively. The maximum velocity along the horizontal (diagonal) axis is estimated to be  $v^{\text{SW,horizontal}} \rightarrow J/2$  ( $v^{\text{SW,diagonal}} \rightarrow J/\sqrt{2}$ ) for  $\Gamma \rightarrow \infty$ . On the other hand, for both axes, it approaches the value  $J$  ( $v^{\text{SW,horizontal}}, v^{\text{SW,diagonal}} \rightarrow J$ ) for  $\Gamma \rightarrow \Gamma_c^{\text{classical,2D}} (= 2J)$ .

The group velocity in 2D obtained by the LSWA increases with decreasing the transverse field (see also Sec. IV A). As we will see below, this behavior agrees with that obtained by a high-order series expansion [116–118]. We extract the group velocity from the dispersion relation obtained by the series expansion up to fourth order of  $\lambda = J/(2\Gamma)$  [116–118]. The dispersion relation is described as

$$\Omega_{\mathbf{k}}^{\text{series}} = \Gamma \left[ \lambda \cdot (-2)\gamma_{\mathbf{k}} + \lambda^2 \cdot (-2)\gamma_{\mathbf{k}}^2 + \lambda^3 \left( \frac{5}{2}\gamma_{\mathbf{k}} - 4\gamma_{\mathbf{k}}^3 \right) + \lambda^4 (7\gamma_{\mathbf{k}}^2 - 10\gamma_{\mathbf{k}}^4) + \mathcal{O}(\lambda^5) \right] + \text{const.}, \quad (\text{B50})$$

where the constant term does not depend on  $\mathbf{k}$  (but depends on  $\lambda$  and  $\Gamma$ ). Note that this relation is consistent with that in Eq. (B46) for  $z = 4$  on a square lattice. We calculate the velocity  $v^{\text{series}} = \max_{\mathbf{k}} \nabla_{\mathbf{k}} \Omega_{\mathbf{k}}^{\text{series}}$  numerically and compare it with our result obtained by the LSWA. As shown in Fig. 23, at a fixed transverse field, the velocity along the horizontal axis obtained by the series expansion increases monotonically as higher-order terms are taken into account. They are always slower than the velocity obtained by the LSWA. On the other hand, both velocities obtained by the LSWA and the series expansion nearly coincide for strong transverse fields. They increase with decreasing the transverse field.

- 
- [1] A. Browaeys and T. Lahaye, *Nat. Phys.* **16**, 132 (2020).  
[2] M. Morgado and S. Whitlock, *AVS Quantum Sci.* **3**, 023501 (2021).  
[3] X. Wu, X. Liang, Y. Tian, F. Yang, C. Chen, Y.-C. Liu, M. K. Tey, and L. You, *Chin. Phys. B* **30**, 020305 (2021).  
[4] P. Scholl, M. Schuler, H. J. Williams, A. A. Eberharter, D. Barredo, K.-N. Schymik, V. Lienhard, L.-P. Henry, T. C. Lang, T. Lahaye, A. M. Läuchli, and A. Browaeys, *Nature* **595**, 233 (2021).  
[5] D. Bluvstein, A. Omran, H. Levine, A. Keesling, G. Semeghini, S. Ebadi, T. T. Wang, A. A. Michailidis, N. Maskara, W. W. Ho, S. Choi, M. Serbyn, M. Greiner, V. Vuletić, and M. D. Lukin, *Science* **371**, 1355 (2021).  
[6] S. Ebadi, T. T. Wang, H. Levine, A. Keesling, G. Semeghini, A. Omran, D. Bluvstein, R. Samajdar, H. Pichler, W. W. Ho, S. Choi, S. Sachdev, M. Greiner, V. Vuletić, and M. D. Lukin, *Nature* **595**, 227 (2021).  
[7] H. Bernien, S. Schwartz, A. Keesling, H. Levine, A. Omran, H. Pichler, S. Choi, A. S. Zibrov, M. Endres, M. Greiner, V. Vuletić, and M. D. Lukin, *Nature* **551**, 579 (2017).  
[8] A. Keesling, A. Omran, H. Levine, H. Bernien, H. Pichler, S. Choi, R. Samajdar, S. Schwartz, P. Silvi, S. Sachdev, P. Zoller, M. Endres, M. Greiner, V. Vuletić, and M. D. Lukin, *Nature* **568**, 207 (2019).

- [9] S. de Léséleuc, V. Lienhard, P. Scholl, D. Barredo, S. Weber, N. Lang, H. P. Büchler, T. Lahaye, and A. Browaeys, *Science* **365**, 775 (2019).
- [10] R. Verresen, M. D. Lukin, and A. Vishwanath, *Phys. Rev. X* **11**, 031005 (2021).
- [11] G. Semeghini, H. Levine, A. Keesling, S. Ebadi, T. T. Wang, D. Bluvstein, R. Verresen, H. Pichler, M. Kalinowski, R. Samajdar, A. Omran, S. Sachdev, A. Vishwanath, M. Greiner, V. Vuletic, and M. D. Lukin, *Science* **374**, 1242 (2021).
- [12] R. Samajdar, W. W. Ho, H. Pichler, M. D. Lukin, and S. Sachdev, *Phys. Rev. Lett.* **124**, 103601 (2020).
- [13] R. Samajdar, W. W. Ho, H. Pichler, M. D. Lukin, and S. Sachdev, *Proc. Natl. Acad. Sci. U.S.A.* **118**, e2015785118 (2021).
- [14] X. Wang, M. H. Christensen, E. Berg, and R. M. Fernandes, *Ann. Phys.* **435**, 168522 (2021).
- [15] Y. D. Liao, H. Li, Z. Yan, H.-T. Wei, W. Li, Y. Qi, and Z. Y. Meng, *Phys. Rev. B* **103**, 104416 (2021).
- [16] V. Lienhard, S. de Léséleuc, D. Barredo, T. Lahaye, A. Browaeys, M. Schuler, L.-P. Henry, and A. M. Läuchli, *Phys. Rev. X* **8**, 021070 (2018).
- [17] R. Kaneko, Y. Douda, S. Goto, and I. Danshita, *J. Phys. Soc. Jpn.* **90**, 073001 (2021).
- [18] M. Yue, Z. Wang, B. Mukherjee, and Z. Cai, *Phys. Rev. B* **103**, L201113 (2021).
- [19] E. Merali, I. J. S. D. Vlugt, and R. G. Melko, *arXiv:2107.00766*.
- [20] E. Guardado-Sanchez, P. T. Brown, D. Mitra, T. Devakul, D. A. Huse, P. Schauß, and W. S. Bakr, *Phys. Rev. X* **8**, 021069 (2018).
- [21] E. H. Lieb and D. W. Robinson, *Commun. Math. Phys.* **28**, 251 (1972).
- [22] M. B. Hastings, *arXiv:1008.5137*.
- [23] Z. Wang and K. R. A. Hazzard, *PRX Quantum* **1**, 010303 (2020).
- [24] B. Blaß and H. Rieger, *Sci. Rep.* **6**, 38185 (2016).
- [25] M. Schmitt and M. Heyl, *SciPost Phys.* **4**, 013 (2018).
- [26] M. Schmitt and M. Heyl, *Phys. Rev. Lett.* **125**, 100503 (2020).
- [27] I. L. Gutiérrez and C. B. Mendl, *Quantum* **6**, 627 (2022).
- [28] M. Schmitt, M. M. Rams, J. Dziarmaga, M. Heyl, and W. H. Zurek, *Sci. Adv.* **8**, eabl6850 (2022).
- [29] M. Schmitt and M. Reh, *SciPost Phys. Codebases* , 2 (2022).
- [30] S.-H. Lin and F. Pollmann, *Phys. Status Solidi B* **259**, 2100172 (2022).
- [31] K. Donatella, Z. Denis, A. L. Boité, and C. Ciuti, *arXiv:2209.03241*.
- [32] E. Granet, M. Fagotti, and F. H. L. Essler, *SciPost Phys.* **9**, 33 (2020).
- [33] I. G. White, B. Sundar, and K. R. A. Hazzard, *arXiv:1710.07696*.
- [34] J. Richter, T. Heitmann, and R. Steinigeweg, *SciPost Phys.* **9**, 31 (2020).
- [35] J. Gan and K. R. A. Hazzard, *Phys. Rev. A* **102**, 013318 (2020).
- [36] U. Schollwöck, *Ann. Phys.* **326**, 96 (2011).
- [37] J. Haegeman, C. Lubich, I. Oseledets, B. Vandereycken, and F. Verstraete, *Phys. Rev. B* **94**, 165116 (2016).
- [38] T. Hashizume, J. C. Halimeh, and I. P. McCulloch, *Phys. Rev. B* **102**, 035115 (2020).
- [39] T. Hashizume, I. P. McCulloch, and J. C. Halimeh, *Phys. Rev. Research* **4**, 013250 (2022).
- [40] A. Kshetrimayum, H. Weimer, and R. Orús, *Nat. Commun.* **8**, 1291 (2017).
- [41] P. Czarnik, J. Dziarmaga, and P. Corboz, *Phys. Rev. B* **99**, 035115 (2019).
- [42] C. Hubig and J. I. Cirac, *SciPost Phys.* **6**, 31 (2019).
- [43] J. Dziarmaga, *Phys. Rev. B* **104**, 094411 (2021).
- [44] J. Dziarmaga, *Phys. Rev. B* **106**, 014304 (2022).
- [45] S.-H. Lin, M. P. Zaletel, and F. Pollmann, *Phys. Rev. B* **106**, 245102 (2022).
- [46] P. Pfeuty, *Ann. Phys.* **57**, 79 (1970).
- [47] H. Rieger and N. Kawashima, *Eur. Phys. J. B* **9**, 233 (1999).
- [48] H. W. J. Blöte and Y. Deng, *Phys. Rev. E* **66**, 066110 (2002).
- [49] S. Bravyi, M. B. Hastings, and F. Verstraete, *Phys. Rev. Lett.* **97**, 050401 (2006).
- [50] P. Calabrese, F. H. L. Essler, and M. Fagotti, *Phys. Rev. Lett.* **106**, 227203 (2011).
- [51] M. Cheneau, P. Barmettler, D. Poletti, M. Endres, P. Schauß, T. Fukuhara, C. Gross, I. Bloch, C. Kollath, and S. Kuhr, *Nature* **481**, 484 (2012).
- [52] P. Jurcevic, B. P. Lanyon, P. Hauke, C. Hempel, P. Zoller, R. Blatt, and C. F. Roos, *Nature* **511**, 202 (2014).
- [53] Z. Gong and R. Hamazaki, *Int. J. Mod. Phys. B* **36**, 2230007 (2022).
- [54] P. Barmettler, D. Poletti, M. Cheneau, and C. Kollath, *Phys. Rev. A* **85**, 053625 (2012).
- [55] J. Despres, L. Villa, and L. Sanchez-Palencia, *Sci. Rep.* **9**, 4135 (2019).
- [56] Y. Takasu, T. Yagami, H. Asaka, Y. Fukushima, K. Nagao, S. Goto, I. Danshita, and Y. Takahashi, *Sci. Adv.* **6**, eaba9255 (2020).
- [57] E. Lieb, T. Schultz, and D. Mattis, *Ann. Phys.* **16**, 407 (1961).
- [58] E. Barouch and B. M. McCoy, *Phys. Rev. A* **3**, 786 (1971).
- [59] S. Sachdev, *Quantum Phase Transitions. Second edition* (Cambridge University press, Cambridge, U.K., 2011).
- [60] P. Calabrese, F. H. Essler, and M. Fagotti, *J. Stat. Mech.* **2012**, P07016 (2012).
- [61] P. Calabrese, F. H. Essler, and M. Fagotti, *J. Stat. Mech.* **2012**, P07022 (2012).
- [62] S. Suzuki, J.-i. Inoue, and B. K. Chakrabarti, *Quantum Ising Phases and Transitions in Transverse Ising Models* (Springer, Berlin/Heidelberg, 2013).
- [63] M. Wimmer, *ACM Transactions on Mathematical Software (TOMS)* **38**, 1 (2012).
- [64] L.-P. Henry, P. C. W. Holdsworth, F. Mila, and T. Roscilde, *Phys. Rev. B* **85**, 134427 (2012).
- [65] L. Cevolani, G. Carleo, and L. Sanchez-Palencia, *New J. Phys.* **18**, 093002 (2016).
- [66] A. S. Buyskikh, M. Fagotti, J. Schachenmayer, F. Essler, and A. J. Daley, *Phys. Rev. A* **93**, 053620 (2016).
- [67] R. Menu and T. Roscilde, *Phys. Rev. B* **98**, 205145 (2018).
- [68] R. Menu and T. Roscilde, *arXiv:2301.01363*.
- [69] M. A. Martín-Delgado, M. Roncaglia, and G. Sierra, *Phys. Rev. B* **64**, 075117 (2001).
- [70] F. Verstraete and J. I. Cirac, *arXiv:cond-mat/0407066*.
- [71] F. Verstraete and J. I. Cirac, *Phys. Rev. A* **70**, 060302(R) (2004).
- [72] F. Verstraete, V. Murg, and J. I. Cirac, *Adv. Phys.* **57**,

- 143 (2008).
- [73] J. Jordan, R. Orús, G. Vidal, F. Verstraete, and J. I. Cirac, *Phys. Rev. Lett.* **101**, 250602 (2008).
- [74] H. N. Phien, J. A. Bengua, H. D. Tuan, P. Corboz, and R. Orús, *Phys. Rev. B* **92**, 035142 (2015).
- [75] R. Orús, *Ann. Phys.* **349**, 117 (2014).
- [76] R. Orús, *Nat. Rev. Phys.* **1**, 538 (2019).
- [77] Y. Hieida, K. Okunishi, and Y. Akutsu, *New J. Phys.* **1**, 7 (1999).
- [78] K. Okunishi and T. Nishino, *Prog. Theor. Phys.* **103**, 541 (2000).
- [79] T. Nishino, Y. Hieida, K. Okunishi, N. Maeshima, Y. Akutsu, and A. Gendiar, *Prog. Theor. Phys.* **105**, 409 (2001).
- [80] N. Maeshima, Y. Hieida, Y. Akutsu, T. Nishino, and K. Okunishi, *Phys. Rev. E* **64**, 016705 (2001).
- [81] Y. Nishio, N. Maeshima, A. Gendiar, and T. Nishino, [arXiv:cond-mat/0401115](https://arxiv.org/abs/cond-mat/0401115).
- [82] H. C. Jiang, Z. Y. Weng, and T. Xiang, *Phys. Rev. Lett.* **101**, 090603 (2008).
- [83] H. F. Trotter, *Proc. Amer. Math. Soc.* **10**, 545 (1959).
- [84] M. Suzuki, *J. Phys. Soc. Jpn.* **21**, 2274 (1966).
- [85] M. Suzuki, *Prog. Theor. Phys.* **56**, 1454 (1976).
- [86] TeNeS: <https://github.com/issp-center-dev/tenes>.
- [87] pTNS: <https://github.com/tsuyoshiokubo/ptns>.
- [88] Y. Motoyama, T. Okubo, K. Yoshimi, S. Morita, T. Kato, and N. Kawashima, *Comput. Phys. Commun.* **279**, 108437 (2022).
- [89] T. Nishino and K. Okunishi, *J. Phys. Soc. Jpn.* **65**, 891 (1996).
- [90] T. Nishino and K. Okunishi, *J. Phys. Soc. Jpn.* **66**, 3040 (1997).
- [91] T. Nishino, T. Hikihara, K. Okunishi, and Y. Hieida, *Int. J. Mod. Phys. B* **13**, 1 (1999).
- [92] R. Orús and G. Vidal, *Phys. Rev. B* **80**, 094403 (2009).
- [93] P. Corboz, J. Jordan, and G. Vidal, *Phys. Rev. B* **82**, 245119 (2010).
- [94] P. Corboz, S. R. White, G. Vidal, and M. Troyer, *Phys. Rev. B* **84**, 041108(R) (2011).
- [95] P. Corboz, T. M. Rice, and M. Troyer, *Phys. Rev. Lett.* **113**, 046402 (2014).
- [96] C. Kollath, A. M. Läuchli, and E. Altman, *Phys. Rev. Lett.* **98**, 180601 (2007).
- [97] A. M. Läuchli and C. Kollath, *J. Stat. Mech.* **2008**, P05018 (2008).
- [98] S. Goto and I. Danshita, *Phys. Rev. B* **99**, 054307 (2019).
- [99] M. Kunimi and I. Danshita, *Phys. Rev. A* **104**, 043322 (2021).
- [100] R. Yoshii, S. Yamashika, and S. Tsuchiya, *J. Phys. Soc. Jpn.* **91**, 054601 (2022).
- [101] P. Weinberg and M. Bukov, *SciPost Phys.* **2**, 003 (2017).
- [102] P. Weinberg and M. Bukov, *SciPost Phys.* **7**, 20 (2019).
- [103] A. W. Sandvik, *AIP Conf. Proc.* **1297**, 135 (2010).
- [104] N. J. Higham and A. H. Al-Mohy, *Acta Numer.* **19**, 159 (2010).
- [105] A. H. Al-Mohy and N. J. Higham, *SIAM journal on scientific computing* **33**, 488 (2011).
- [106] C. de Boor, *A Practical Guide to Splines* (Springer, New York, 1978).
- [107] F. Iglói and H. Rieger, *Phys. Rev. Lett.* **85**, 3233 (2000).
- [108] D. A. Huse, *Phys. Rev. B* **37**, 2380 (1988).
- [109] C. M. Soukoulis, S. Datta, and Y. H. Lee, *Phys. Rev. B* **44**, 446 (1991).
- [110] K. J. Runge, *Phys. Rev. B* **45**, 7229 (1992).
- [111] K. Nagao, M. Kunimi, Y. Takasu, Y. Takahashi, and I. Danshita, *Phys. Rev. A* **99**, 023622 (2019).
- [112] R. Kaneko and I. Danshita, *Commun. Phys.* **5**, 65 (2022).
- [113] P. Pfeuty and R. Elliott, *J. Phys. C: Solid State Phys.* **4**, 2370 (1971).
- [114] A. A. Ovchinnikov, D. V. Dmitriev, V. Y. Krivnov, and V. O. Chervanovskii, *Phys. Rev. B* **68**, 214406 (2003).
- [115] Y. Kato and T. Misawa, *Phys. Rev. B* **92**, 174419 (2015).
- [116] J. Oitmaa, C. Hamer, and W. Zheng, *Series Expansion Methods for Strongly Interacting Lattice Models* (Cambridge University Press, 2006).
- [117] C. J. Hamer, J. Oitmaa, Z. Weihong, and R. H. McKenzie, *Phys. Rev. B* **74**, 060402(R) (2006).
- [118] C. J. Hamer, J. Oitmaa, and W. Zheng, *Phys. Rev. B* **74**, 174428 (2006).